Modelling and simulation of Proton Exchange Membrane fuel cell with serpentine bipolar plate using MATLAB

Awotwe, Tabbi Wilberforce; El-Hassan, Zaki; Khatib, F. N.; Al Makky, Ahmed; Baroutaji, Ahmad; Carton, James G.; Thompson, James; Olabi, Abdul-Ghani

Published in:
International Journal of Hydrogen Energy

DOI:
10.1016/j.ijhydene.2017.06.091

Published: 05/10/2017

Document Version
Peer reviewed version

Modelling and Simulation of Proton Exchange Membrane Fuel cell with Serpentine bipolar plate using MATLAB

Tabbi Wilberforce[1], Zaki El-Hassan[1], F. N. Khatib[1], Ahmed Al Makky[1], Ahmad Baroutaji[2], James G. Carton[3], James Thompson[1], Abdul G. Olabi[1]

1. Institute of Engineering and Energy Technologies, University of the West of Scotland, UK
2. School of Engineering, Faculty of Science and Engineering, University of Wolverhampton, UK
3. School of Mechanical & Manufacturing Engineering, Dublin City University, Dublin, Ireland

Abstract

This report presents experimental results derived from a Proton exchange Membrane fuel cell with a serpentine flow plate design. The investigation seeks to explore the effects of some parameters like cell operational temperature, humidification and atmospheric pressure on the general performance and efficiency of PEM fuel cell using MATLAB. A number of codes were written to generate the polarization curve for a single stack and five (5) cell stack fuel cell at various operating conditions. Detailed information of hydrogen and oxygen consumption and the effect they have on the fuel cell performance were critically analysed. The investigation concluded that the open circuit voltage generated was less than the theoretical voltage predicted in the literature. It was also noticed that an increase in current or current density reduced the voltage derived from the fuel cell stack. The experiment also clearly confirmed that when more current is being drawn from the fuel cell, more water will also be generated at the cathode section of the cell hence the need for an effective water management to improve the performance of the fuel cell. Other parameters like the stack efficiency and power density were also analysed using the experimental results obtained.

Key words: PEM Fuel cell, MATLAB, Polarization curve, Voltage, Current

Introduction

Energy is the backbone of any modern society. It forms the hub that determines the survival of all living creatures [1]. Fossil fuel has powered the economies of the developed world since the industrial revolution [2]. This in effect has led to elevated levels of prosperity and the general welfare of human society on earth. The high depletion of petroleum based energy resources and the environmental pollution and climate change caused by the burning of fossil

fuel has raised many concerns for the need to look for alternatives to generate energy for society. A fuel cell is an electro-chemical power source that transforms chemical energy in fuel, directly into electrical energy. However unlike most electrical power sources like the batteries which store their reactants within a cell, the reactants of the fuel cell are normally stored externally. The electrodes in a fuel cell are not consumed as in battery -irreversibly in a primary cell and reversibly in a secondary cell- and do not take part in the reaction. Fuel cells are already in use to produce electricity for small portable applications, and more recently being used for stationary applications such as emergency power generators [1-3].

A fuel cell is made up of negatively charged electrode (Anode), a positively charged electrode (Cathode) and an electrolyte membrane [4]. Protons are carried from the anode to the cathode through the electrolytic membrane and the electrons are carried to the cathode over an external circuit. In real life situations, it is impossible for molecules to stay in an ionic state hence they merge with other molecules in order to return to the neutral state. Hydrogen protons found in the fuel cells often stay in the ionic state by travelling from molecule to molecule and diffusing through the membrane. The PEM Fuel cells depicted in Fig. 1 function through the principle of an electrochemical reaction between hydrogen and oxygen in the presence of a platinum catalyst. Reactive gases are carried through the fuel cell through the anode and the cathode. The anode serves as the path where the hydrogen travels through to the reactive site. The hydrogen on the anode eventually converges on the membrane electrode assembly (MEA) which has the platinum catalyst deposited on it. The hydrogen is split into a proton and an electron at the anode [2], the cathode serves as the collective site where the electrons that could not pass through the MEA eventually meet to form water. MEA is only permeable to protons and not to electrons. The electrons that failed to pass through the MEA then pass through an external circuit producing the current [3].

Figure 1: Serpentine PEM fuel cell with 11.56cm^2 active area

In order for a fuel cell to produce electricity effectively and efficiently, the cell must be supplied continuously with the fuel and oxidant [4]. The product water must be well controlled and removed as it build up tends to reduce the efficiency of the fuel cell.

There are several losses that are experienced during the process. These are activation losses, ohmic losses and mass transport losses. Mass transport is defined as the flow of species and this have negative effect on the performance of the fuel cell [5-7]. Losses caused by mass transport are called concentration losses. The electrolyte layer is also another important region of the fuel cell. The electrolyte layer is essential for a fuel cell to work properly. In PEM fuel cells (PEMFCs), the fuel travels to the catalyst layer and is then split into protons (H^+) and electrons. Electricity is generated as long as the electrons flow through the load [8]. The membrane found in a fuel cell must also meet these requirements: high ionic conductivity, present an adequate barrier to the reactants, be chemically and mechanically stable, low electronic conductivity, ease of manufacturability/availability and preferably of low cost.

Mathematical modelling for PEMFC

The model developed intends to explain the fundamental electrochemical transport characteristics and charge transfer that usually occurs in the fuel cell. These mathematical models can best be used to describe the phenomenon occurring in the fuel cell, predict the fuel cell performance under different operating conditions and optimize the design of the fuel cell. The results obtained mathematically were compared to the experimental results.

Thermodynamic performance of the fuel cell

The anodic reaction leads to the hydrogen gas breaking into protons and electrons. The electrochemical reaction takes place on the catalyst layer that is made of platinum as shown in equation 1 [9].

$$2H_{2(g)} \rightarrow 4H^+ + 4e^- \quad (1)$$

The released electrons are not permeable to the proton exchange membrane hence only the protons are able to go through the membrane whiles the electrons go through an external load where electrical work is done and then flow back to the cathode. The protons or hydrogen ions move to the cathode section of the fuel cell where it meets the oxygen and the electrons from the external circuit forming water from equation 2.

$$4H^+ + 4e^- + O_2 \rightarrow 2H_2O_{(l)} \quad (2)$$

The entire chemical reaction can be summarised in Eq. (3):

$$2H_{2(g)} + O_{2(g)} \rightarrow 2H_2O_{(l)} \quad (3)$$

The overall reaction in Eq. (3) could be likened to combustion with hydrogen being the reacting fuel. Combustion is considered as an exothermic process hence there is significant release of energy and the Eq. (4) shows the chemical equation for an exothermic reaction.

$$2H_{2(g)} + O_{2(g)} \rightarrow 2H_2O_{(l)} \ + Heat \quad (4)$$

The difference between the heat of formation of products and reactants is the enthalpy of the reaction. Therefore the enthalpy of reaction for the entire process is given by Eq. (5):

$$\Delta H_r = \Delta H_f(H_2O) - \left(\Delta H_f(H_2) + \frac{1}{2}\Delta H_f(O_2)\right) \quad (5)$$

At a temperature of 25°C the heat of formation of liquid water is -286 kJ/mol. The negative sign signifies that the reaction is exothermic with heat being released into the surroundings.

Theoretical Fuel cell Potential

The conversion of the free energy change in chemical reaction directly into electrical energy is described as the electrochemical energy conversion. It is also the free energy change which is the maximum theoretical electrical work (W_{elec}) a system can perform at any given constant temperature and pressure from a given reaction. This limiting value can be expressed in molar quantities as:

$$W_{elect} = -\Delta G \quad (6)$$

The Gibbs free energy (ΔG) is the energy required for a system at a constant temperature with negligible volume, minus any energy transferred to the environment due to heat flux. The general electrical work is a product of charge and potential:

$$W_{el} = qE \quad (7)$$

Where W_{el} = electrical work ($Jmol^{-1}$)

Q = charge (Coulombs mol^{-1})

E = potential (Volts)

The total charge (q) from any fuel cell reaction is given by:

$$q = nN_{Avg}q_{el} \tag{8}$$

but $N_{Avg}\, q_{el} = F$.

$$q = nF \tag{9}$$

Where n is the number of electrons per molecule of H_2 (2), N_{Avg} is the number of molecules per mole (Avogadro's number) (6.022×10^{23} molecule/mol) and q_{el} is the charge of 1 electron (1.602×10^{-19} Coulombs/electron).

Faradays constant (F) which is shown in Eq. (9) is the product of Avogadro's number and the charge of 1 electron leading to F = 96,485 Coulombs/electron-mol [11].

$$Electric\ Work\ (W_{el}) = nFE \tag{10}$$

But the maximum amount of electrical energy generated in a fuel cell is equal to the Gibbs free energy, ΔG.

The theoretical potential of a fuel cell is therefore represented in Eq. (11):

$$-\Delta G = nFE \tag{11}$$

$$E = {}^{-\Delta G}/_{nF} \tag{12}$$

The first law of thermodynamics states that energy cannot be created nor destroyed but can only be converted from one form to another [12] hence for a steady–state flow, if the kinetic and potential energies for the species can be neglected and if no temperature difference occurs between the flowing fluids and the cell, the energy balance based on specific quantities per moles is as shown in Eq. (13):

$$Q_{out} - W = -\Delta H \tag{13}$$

$$Q_{Out} - nFE = \left(\Delta H_f\right)_{H_2O} - \left(\Delta H_f\right)_{H_2} - {}^{1}/_{2}\left(\Delta H_f\right)_{O_2} \tag{14}$$

Where:

H = the enthalpy of species in kJ/kmole.

n = numbers of kmoles of species reacting per unit time in kmole/sec

Q_{out} = the amount of heat released in kW

Experimental work

A summary of the properties of the various material utilized in this experimental work is shown in Table 1. The purchased fuel cell supplied by fuel cell store, United States, had five cells with graphite used as the main flow plate material. The gas channel was designed to have a serpentine flow channel and the housing was made of acetyl, a plastic or rubberlike material in order to reduce the overall weight of the fuel cell. The purchased fuel cell is air breathing and had air channels where a fan is attached to help in mass transport and effective distribution of the air as well as help in water removal as shown in Fig. 1.

Figs. 2 and 3 show the stack arrangement and the position of the MEA modelled using solid works.

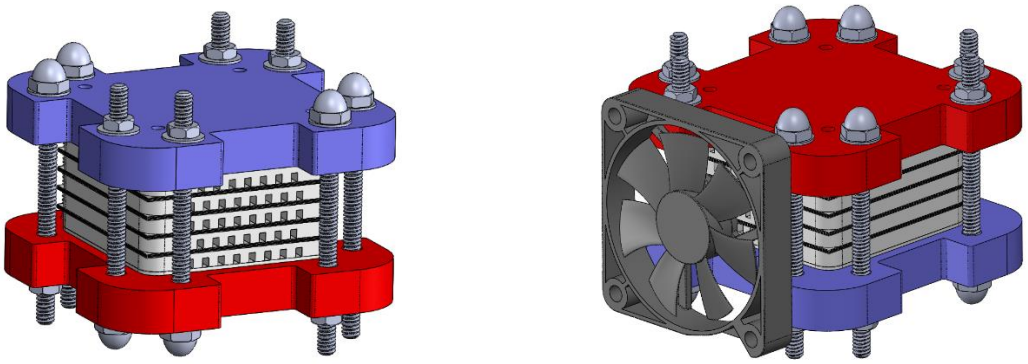

Figure 2: 5 cell stack Proton Exchange Membrane fuel cell

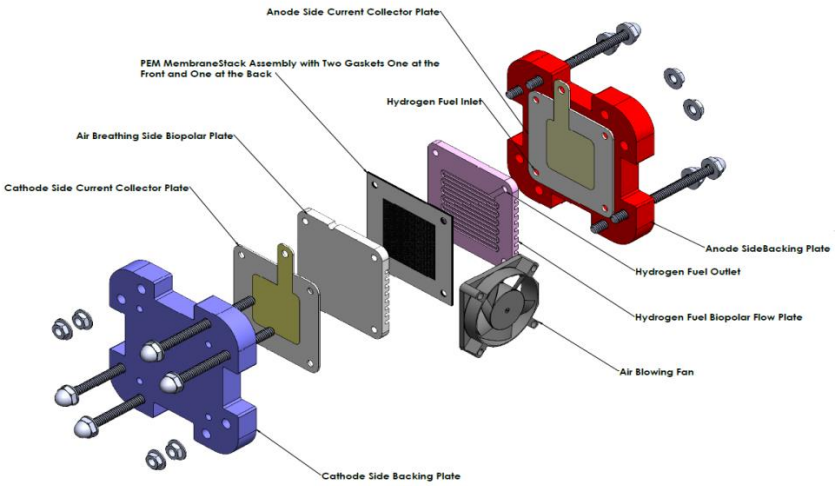

Figure 3: Exploded view of purchased fuel cell

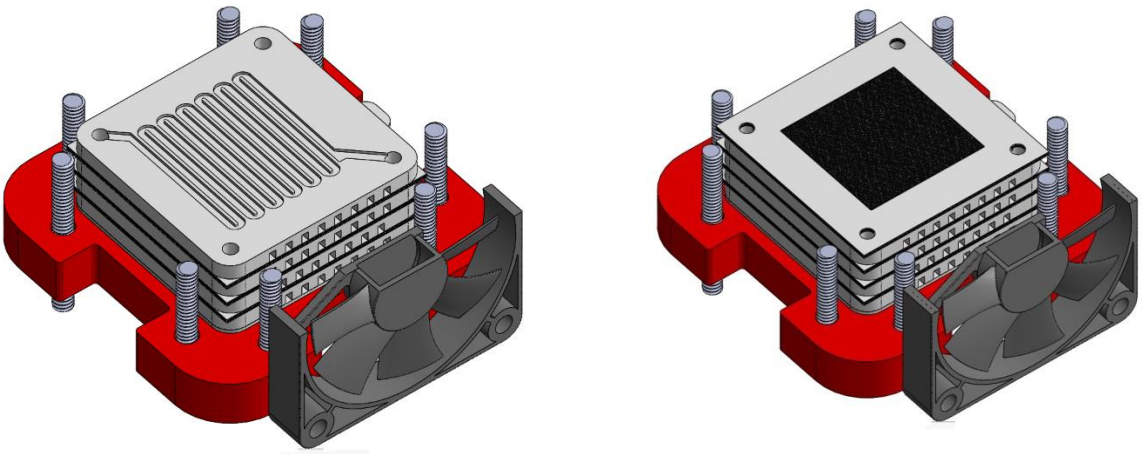

Figure 4: Stack arrangement of purchased fuel cell.

Table 1: Material used for some components in the PEM fuel cell.

FUEL CELL COMPONENT	*MATERIAL*	*PROPERTIES*
HOUSING	Acetyle	Supplier: (Fuel Cell Store)
MEA	Nafion 212	Active area: 3.4cm X 3.4cm Catalyst loading 0.4mg Pt/cm^2) Supplier: Fuel cell store
Flow plate	Graphite (Serpentine design)	24 pores/cm Thickness: 0.65mm Supplier: Fuel Cell Store
Gaskets	Silicon	Thickness: 0.8mm Supplier: Fuel Cell Store

Experimental Set up and procedure

The experimental set up is very similar to Baroutaji et al. [9]. The only difference is the usage of a potentiostat (Gamry Instrument 5000). The potentiostat / galvanostat draws a fixed current from the fuel cell and measures the fuel cell output voltage. By slowly stepping the load on the potentiostat, the voltage response of the fuel cell can be determined. Figs. 5 and 6 show the experimental setup.

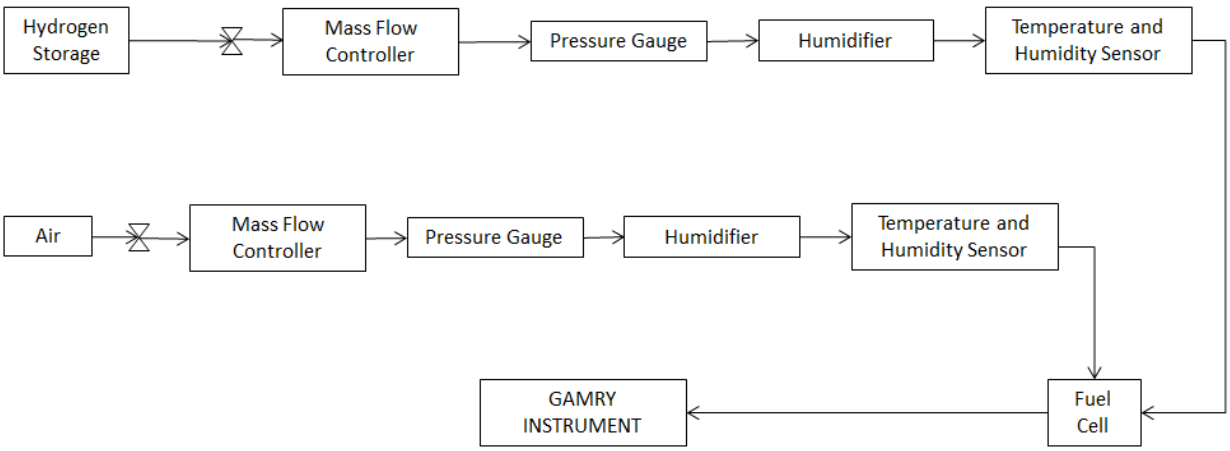

Figure 5: Block diagram showing the various components in the experiment.

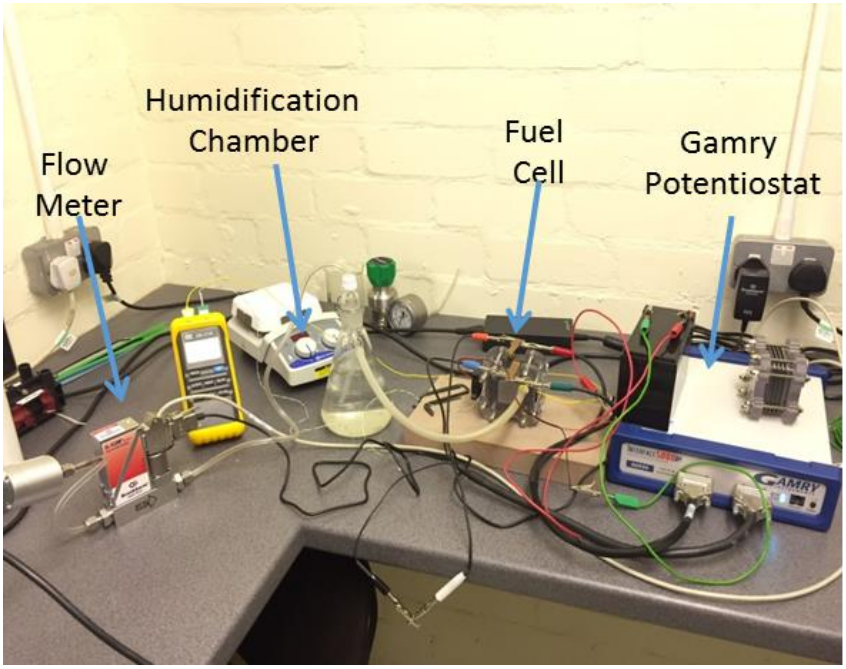

Figure 6. Experimental set up

The experimental setup is shown in Fig 6. The reactant hydrogen gas was produced using a hydrogen generator. The hydrogen generator had a tube with a diameter of 6.54mm that serves as the passage for the hydrogen gas from the generator. The piping system of the hydrogen generator was further linked to the fuel cell through another tubing of diameter 3.685mm. The laboratory pressure was maintained at atmospheric (101.325Pa) and the relative humidity was kept at 70%. The temperature of the lab was 15^{o}C, which is 288K. The air and hydrogen gas were humidified as stated by the manufacturer of the cell in order to improve the characteristic performance of the fuel cell. Humidification of the reactant gases is often done to prevent the portion of the MEA where the gases would be traveling through from drying up. The open circuit voltage was detected by using the potentiostat (Gamry Interface 5000). The Gamry instrument as shown in Fig. 7 is an instrument for cell level testing of various energy storage and conversion devices and includes capabilities for monitoring both half-cell voltages and the whole cell voltage during an experiment.

Figure 7: The Gamry instrument

In order to conduct an experiment, the setup is tested using a dummy cell. The dummy cell is a circuit board used for calibration and troubleshooting of the potentiostat. There are two (2) test cells equipped with terminals that are aligned on the edges of the circuit boards. Fig. 8 shows the dummy cell for the calibration of the experimental setup.

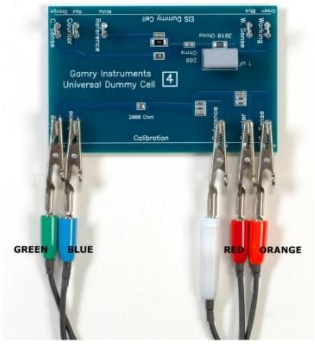

Figure 8: Dummy Cell for Gamry instrument

The circuit is calibrated with a 2 kΩ precision resistor. Potentiostats are not perfectly accurate hence the value of the resistor is often between 1.994KΩ and 2.006KΩ. An AC calibration of

the potentiostat was performed prior to the testing of the fuel cell. Fig. 9 shows the connection of the Gamry instrument to the fuel cell. The coral and red terminals were connected to the anode side of the fuel cell whiles the green and blue terminals were connected to the cathode side of the fuel cell as shown in Fig. 9.

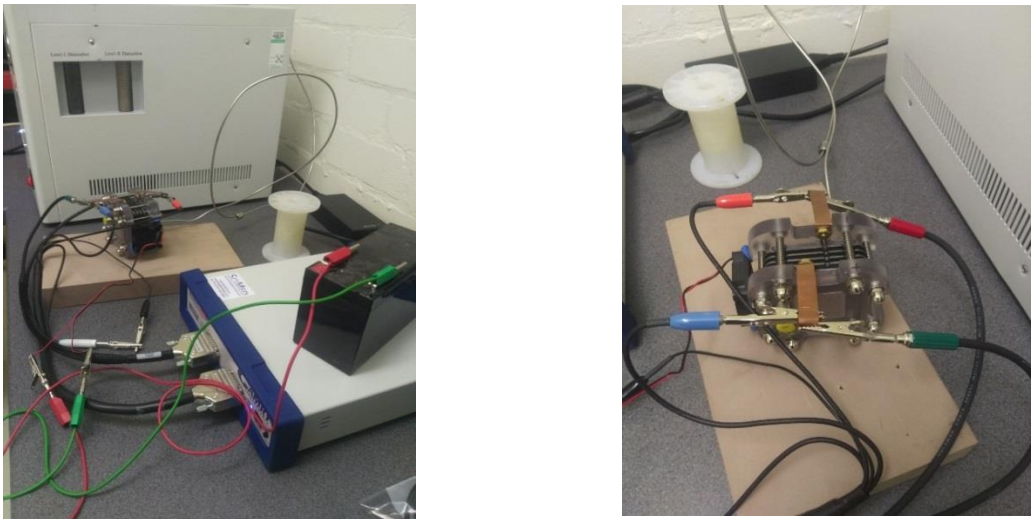

Figure 9: Connection of Gamry Instrument to fuel cell.

The hydrogen generator shown in Fig. 10 was also turned on after the water tank was filled with de-ionized water. It can also be seen that a fan is attached to the fuel cell. The fan is powered by a 12V dc power supply to aid in the mass transport of the fuel cell reactants and products.

Figure 10: Hydrogen generator

A K-type thermocouple was placed at the back of each bipolar plate for the measurement of the temperature. The cell was operated between a temperature of 18°C and 65°C for all experiments. This range is the steady state region where the fluctuations were minimised.

There are several concepts that help in the analysis of fuel cell reactions. Some of these are absolute enthalpy, specific heat and higher and lower heating values [9]. A number of thermodynamic equations were used during the analysis of these experiments to understand and model fuel cell performance since fuel cell transform chemical energy into electrical energy following well established thermodynamic relations. Simple thermodynamic concepts allow and facilitate the prediction of the fuel cell system properties such as potential, temperature, pressure, volume of the gas and its molar concentration in a fuel cell. The heat of formation (h_f) is related to the energy of the chemical bonds and the sensible thermal energy (Δh_s) is the difference in enthalpy between the given conditions and the reference temperature with no phase change. A measure of the amount of heat energy required to increase the temperature of a unit body mass (or mole) by 1^oC is the specific heat per unit mass (or mole) and entropy may be simply considered a measure of the quantity of heat that shows the possibility of conversion into work [9-13]. Gibbs free energy on the other hand is a measure of the amount of useful work obtained from an isothermal, isobaric system when the system changes from a steady state conditions to another. The maximum fuel cell performance can then be observed through the reversible voltage. The net output voltage is the actual fuel cell voltage after activation polarisation and ohmic and concentration losses [14-18]. A number of responses were considered during the course of the experiment. Table 2 shows the various responses that were considered during the investigation.

Table 2: Various responses considered during experimental investigation.

Responses	
Maximum Voltage	V
Maximum Current	A
Current at Intercept of I – V graph	A
Power density at Intercept of I – V graph	W
Maximum Power density	W cm^{-2}
Maximum Voltage efficiency	%
Hydrogen fuel efficiency	%
Hydrogen Consumption	g s^{-1}
Oxygen Consumption	g s^{-1}
Waste Heat generated by stack	W

Ohm's law states that voltage is directly proportional to current depending on the magnitude of resistance as shown in Eq. (15).

$$V = I \times R \tag{15}$$

Where V = voltage of the circuit and I is the current flowing through the circuit.

In instances where the total energy is based upon the higher heating value being converted into electrical energy, a theoretical potential of 1.48V per cell could be attained.

The higher heating value (HHV) is a measure of the amount of heat released (heat of combustion) by a constant quantity of fuel between identical initial and final temperature (25^oC). The temperature of the fuel is often set at 25°C then the fuel is ignited and burnt, then the combustion products are returned to 25^oC. Stopping the cooling at 150^oC often leads to the lower heating value (LHV). The chemical consumption of the fuel affects both the higher and lower heating value [18]. Enthalpy of vaporization is also defined as the difference between higher and lower heating values [19]. A major approach used in determining the performance of a fuel cell often is through a plot of the current and voltage which is commonly referred to as the polarization curve or the I-V curve (Current vs Voltage). As long as a fuel cell is supplied with enough fuel, it should be able to produce good amount of current and maintain a constant voltage that is determined by thermodynamic considerations.

The polarization curve is the best tool for fuel cell characterization and also the easiest approach for testing fuel cells. The polarization curves are often generated using potentiostat/ galvanostat. Slowly stepping the load on the potentiostat, the voltage response of the fuel cell can be determined [20]. Maximum electrical energy output and potential difference between the cathode and the anode are achieved provided the fuel cell is operating under thermodynamically reversible conditions. The theoretical reversible cell potential is the maximum possible cell potential. The net output voltage of a fuel cell at a specific current density is simply the reversible cell potential minus the irreversible potential as shown in Eq. (16).

$$V(i) = V_{rev} - V_{irrev} \tag{16}$$

Where V_{rev} = E_r is the maximum (reversible) voltage of the fuel cell and V_{irrev} is the irreversible voltage loss (over-potential) around the cell. The total electrical work (W_{elec}) a system can perform at a constant temperature and pressure process is given by the Gibbs free energy change for the process as shown in Eq. (17):

$$W_{elec} = -\Delta G \tag{17}$$

The Gibbs free energy can also be defined as the amount of energy needed for a system at a constant temperature with a negligible volume, minus any energy transferred to the environment due to heat flux. Once the temperature and pressure becomes constant, Eq. (18) is valid for fuel cell systems [20-28]:

$$\Delta G = \Delta H - T\Delta S \tag{18}$$

Where ΔG is the Gibbs free energy, H is the heat content (enthalpy of formation), T is the absolute temperature and S is entropy.

According to the second law of thermodynamics, the change in free energy or maximum useful work can be derived when a perfect fuel cell operating irreversibly is dependent upon temperature [21]. Thus, W_{elect}, the electrical power output is:

$$W_{elec} = \Delta G = \Delta H - T\Delta S \tag{19}$$

The reaction enthalpy and entropy depend on temperature. Knowledge of the system temperature and pressure allows the determination of the enthalpy of the system. This is usually done by combining both chemical and thermal bond energy. The heat and mass balance can be used to express the performance of the fuel cell [22] as well as shown in Eq. (20).

$$\Delta H = \sum m_i h_i - \sum m_j h_j \tag{20}$$

$\sum m_i h_i$ is the summation of the mass times the enthalpy of each substance departing from the system whiles $\sum m_j h_j$ is the summation of the mass times the enthalpy of each substance arriving at the system. The potential of a system to perform electrical work by a charge Q through an electrical potential difference is also given by:

$$W_{elec} = EQ \tag{21}$$

The actual work of fuel cell from Eq. (21) is always smaller than the maximum useful work because of irreversibility in the process.

These include activation potential (V_{act}), ohmic overpotential (V_{ohmic}) and concentration over-potential (V_{Conc}). Fig. 11 shows the various losses often experienced inside a fuel cell.

$$V_{irr} = V_{act} + V_{ohmic} + V_{Conc} \tag{22}$$

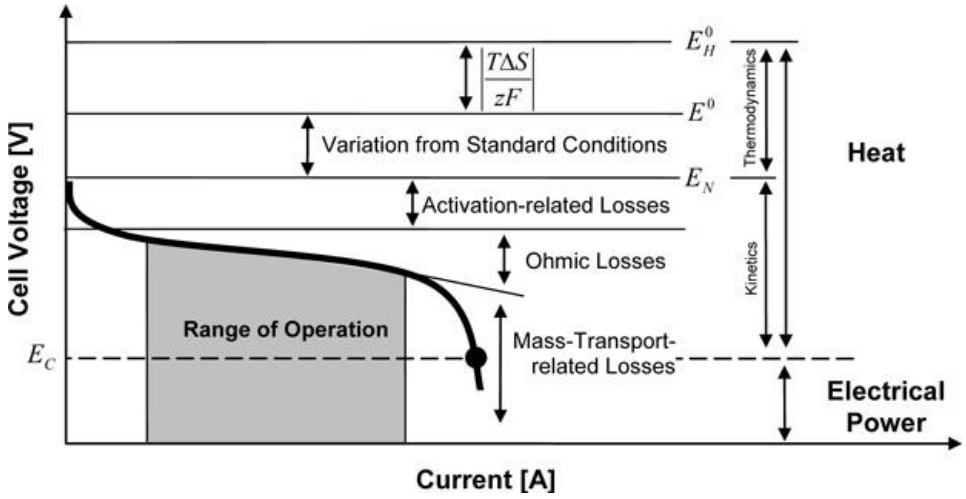

Figure 11: Various losses experienced in a fuel cell [23]

At standard temperature and pressure, the highest voltage that can be derived from hydrogen-oxygen fuel cell is 1.229V [23]. Most fuel cell reactions have theoretical voltages in the 0.8 to 1.1V range. Connecting several cells in series is one of the ways of obtaining a higher voltage. The product of the current measured and the measured voltage at the current often leads to the power being delivered by the fuel cell as shown in Eq. (23):

$$P = I \times V \tag{23}$$

The active area of the MEA being used for this experimental work is 11.56cm^2. This value when divided by the current gives the current density. The power density is obtained by dividing the power by the active area of the fuel cell. Since the purchased fuel cell had five stacks, the current generated by the whole stack divided by the number of stacks of the fuel cell gives the value of current for a single stack. The same method can be used to calculate the power and power density to be obtained from the fuel cell. The voltage efficiency can also be derived as the measured voltage divided by the theoretical maximum voltage of 1.22V [23].

$$\varepsilon_{Voltage} = V_{measured}/V_{theoretical} \tag{24}$$

The fuel efficiency is the measure of the exact percentage of hydrogen feed converted per unit time. There are several inefficiencies in the fuel cell which eventually affects the general performance of the fuel cell as concluded by O'Hayre et al. [24]. It can be calculated by comparing the input flow rate of hydrogen with the measured current from the cell using Eqn. (25):

$$\varepsilon_{fuel} = \left({}^{1}/_{nf}\right)/V_{fuel} \tag{25}$$

Analysis of results

A number of codes were written in MATLAB to facilitate the generation of polarization curves of the various responses. The codes were done to generate results for both a single stack and the five cells stack fuel cell.

The first polarization curve was for the voltage and current for the who1e stack as shown in figure 12a. It can be clearly seen that at atmospheric pressure the fuel cell had its highest voltage as 4.49 V and a current of 1.7A. The current density for the whole stack was 0.15A/cm^2 and this was also plotted against voltage.

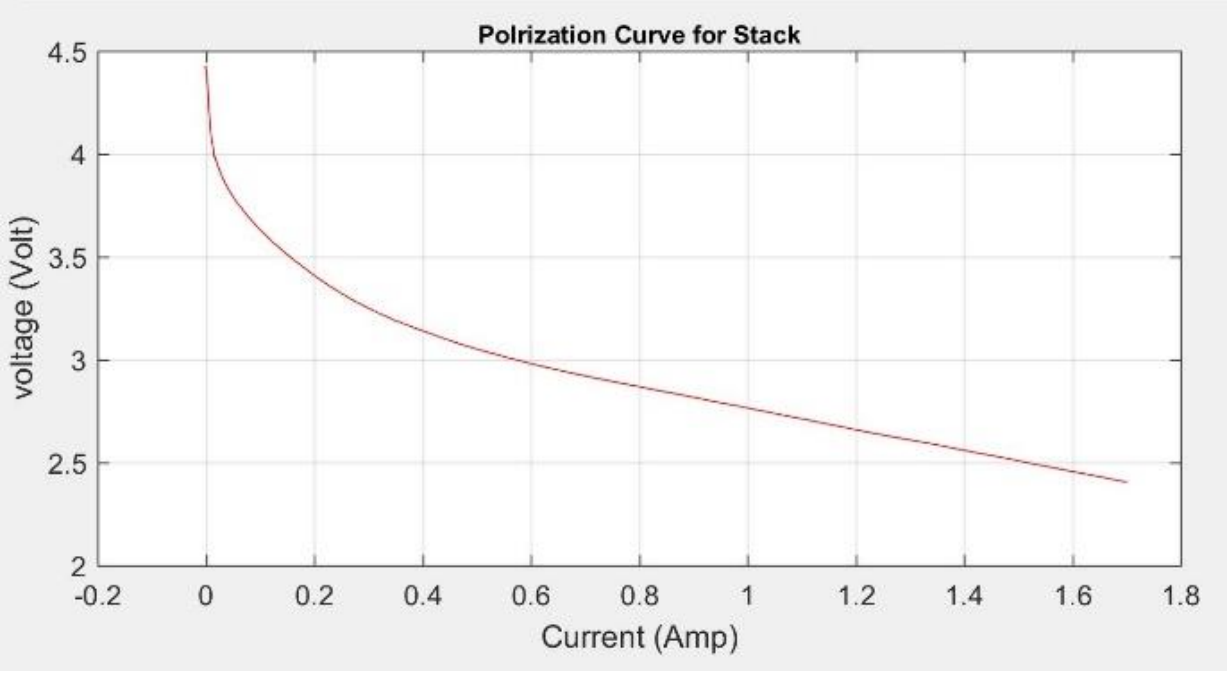

Figure 12a: Polarization curve for the stack serpentine fuel cell

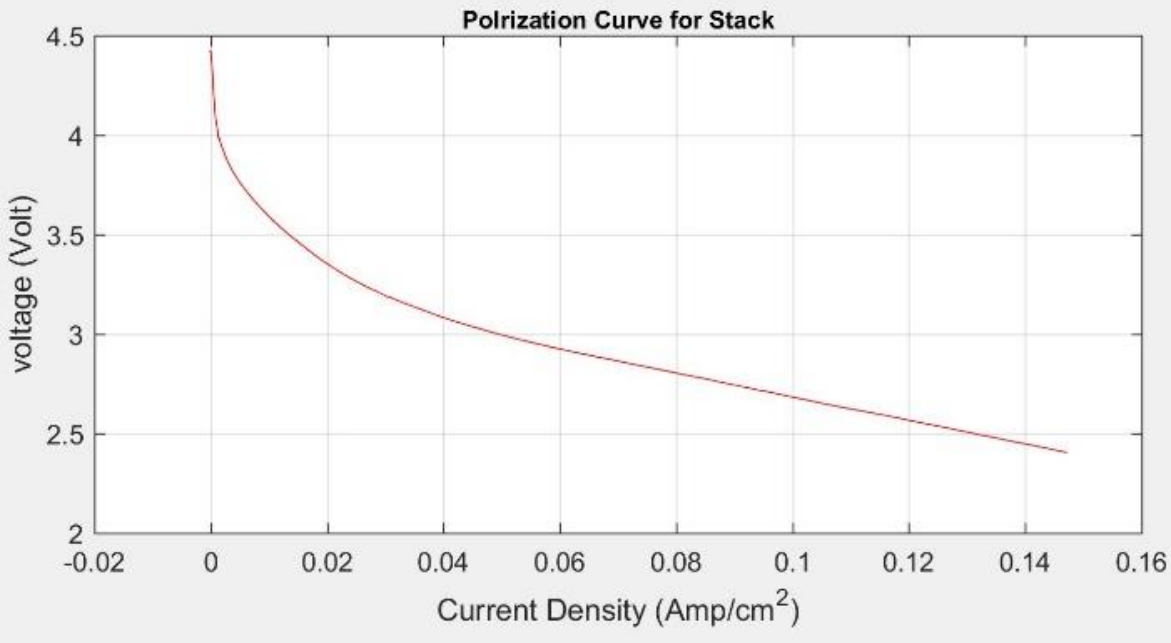

Figure 12b: Polarization curve for the 5 stacks serpentine fuel cell

Dividing the various values of Fig. 12b by five gives the polarization curve for a single stack. The scaled values of voltage, current and current density are shown in Figs. (13a) and (13b). It can be seen that the highest voltage achieved is 0.9V when the fuel cell current is zero. According to literature [23, 25, 26], this value is supposed to be 1.22V but due to the irreversibility in the process the achieved voltage value is lower at 0.9V.

All these electrochemical characteristics are results of activation polarization where the chemical reaction has to overcome an energy barrier which reduces the open circuit voltage of the fuel cell [26]. Once the fuel cell starts producing currents, ohmic losses set in and concentration and/or mass transport losses then add to the losses occurring in the fuel cell resulting in overall loss that leads to the reduced voltage value. As more current is being drawn from the fuel cell, the voltage drops drastically which explains the reason for a huge drop in voltage from 0.9V to nearly 0.5V as the current is increased to 1.7 in Fig. (13a).

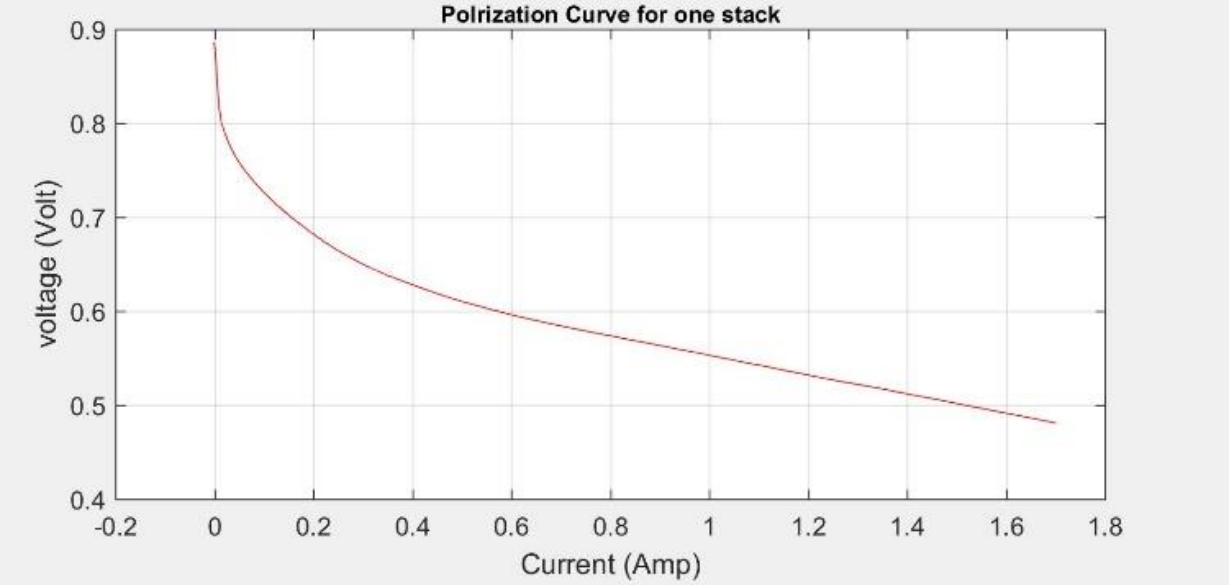

Figure 13a: Polarization curves for a single stack fuel cell - current

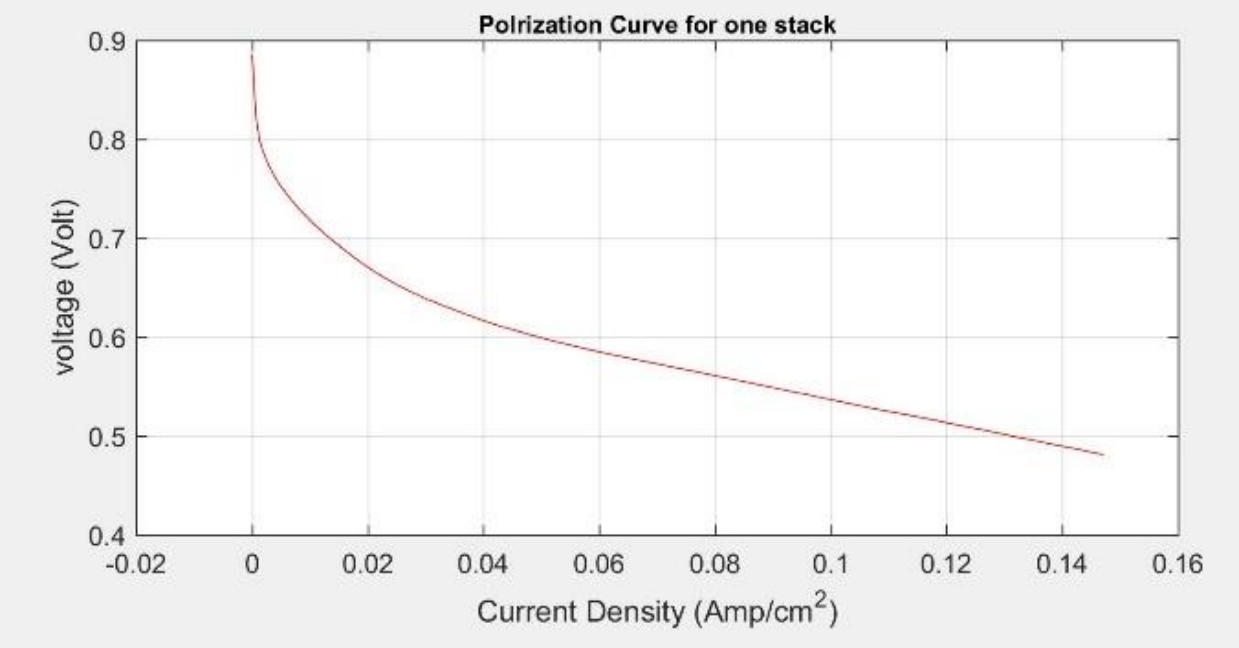

Figure 13b: Polarization curves for a single stack fuel cell – current density

The fuel cell is air breathing and also to increase the voltage of the fuel cell to approach the value reported in the literature, the oxygen flow rate was made higher than the hydrogen flow rate [25]. So while the hydrogen was flowing at a rate of 15ml/min, the oxygen was kept at 150 ml/min. It is also confirmed that as more hydrogen gas is consumed, more current is also produced. It can also be explained that where large amounts of current is being drawn from

the fuel cell, the hydrogen consumption will also increase as shown in Fig. (14a). A similar situation is seen with oxygen. As the current keeps increasing, the oxygen consumption equally increases but this will be dependent on the flow rates at which the gases are travelling and the pressure drop experienced at each electrode. This comes back to the fact that the bipolar plates contributes significantly to the amount of current being generated from the fuel cell.

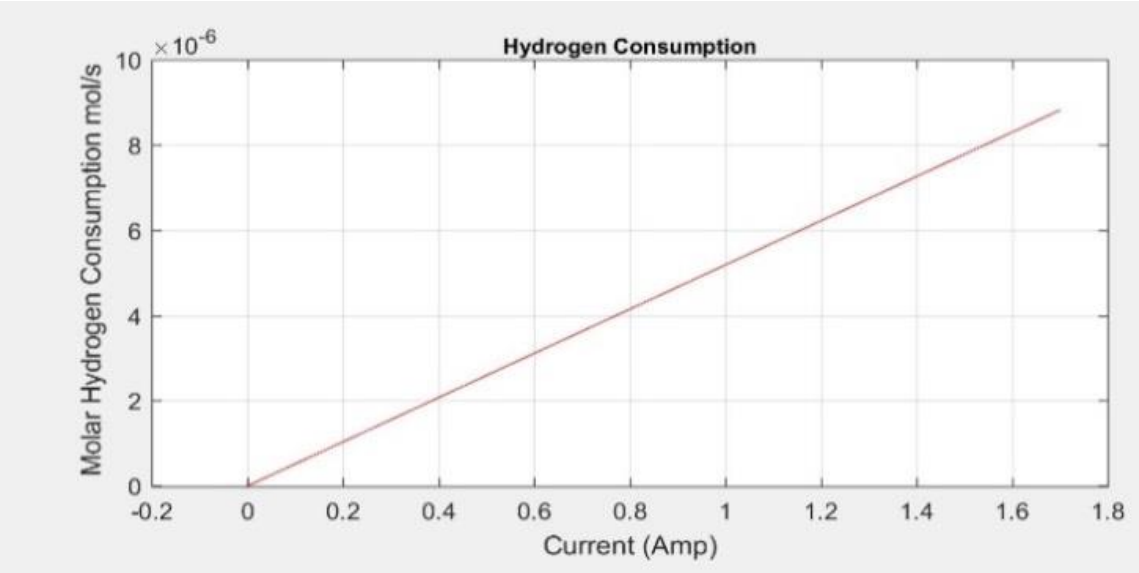

Figure 14a: Various reactant consumption of the whole fuel cell stack

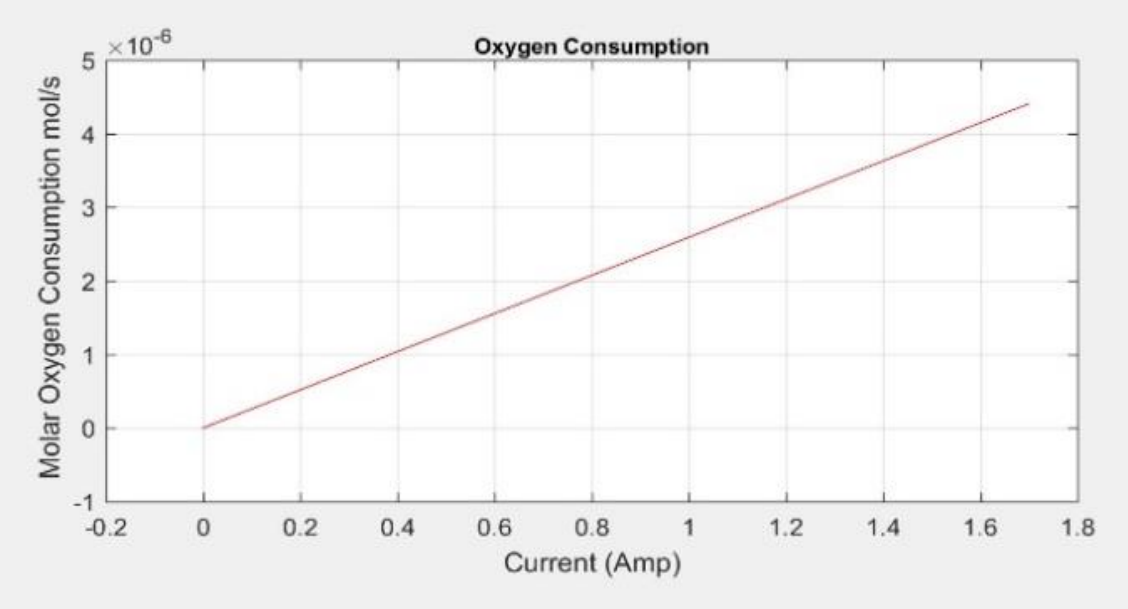

Figure 14b: Various reactant consumption of the whole fuel cell stack

It is worth noting that at equilibrium, the net current should be zero because the reversible reaction is believed to proceed at equal rates in both the forward and the backward directions simultaneously. This is called the exchange current density [26] but when the current density becomes very large that the reactants concentrations fall to zero at the catalyst sites, a limiting current density is produced. A typical limiting current density in a fuel cell is often between 1 to 10A/cm^2 but within a practical cell is it closer to 1A/ cm^2 and there is no way the fuel cell can produce a higher current density than its limiting current density [26].

One of the criteria considered as shown in Fig. 15 is the water management in the fuel cell. To maintain the performance of the fuel cell, the MEA water balance must be maintained and this remains one of the main issues of the PEM fuel cell industry [27]. Too much water in the fuel cell causes the flooding of the cell and the inhibition of the catalyst ability to facilitate the hydrogen-oxygen reaction [26]. It impedes the reactant diffusion to the catalyst sites due to the flooding of the electrodes, gas diffusion backings or even the gas channels if the water removal from the fuel cell is not highly efficient and this decreases the diffusion potentials. The gas temperature usually determines the humidification needed for the experimental work. From the figure below it can be seen that though more water is often produced at the cathode side of the fuel cell, it is proportional to current density. A high current density means high amount of water expected to be produced as a by-product by the fuel cell. Too little water can lead to the drying out of the membrane which will have adverse effects on the fuel cell.

Protonic conductivity of the PEM fuel cell is highly dependent on the water content of the MEA. It decreases in instances when there is less water and this causes the cell resistance to increase as well. Maintenance of appropriate water levels is the main reason for the humidification of the gas before entering the MEA during the process

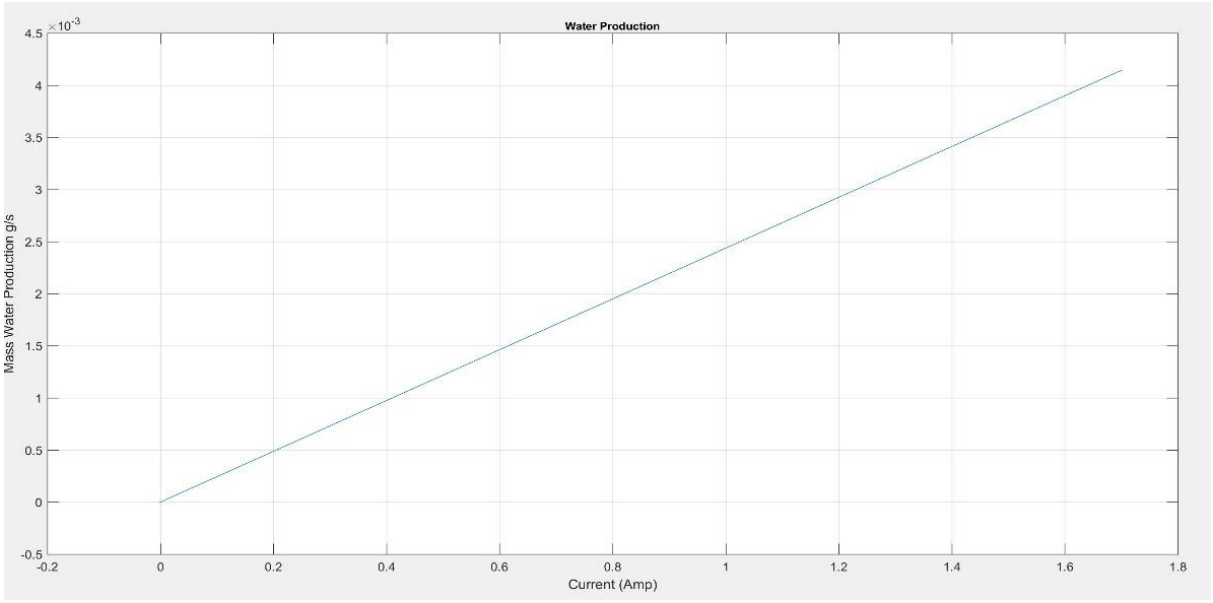

Figure 15: Water production for the entire fuel cell.

As explained earlier the product of the current and voltage generates the expected power from the fuel cell. It can also be seen that as the current increases, the power increases as well and it is shown on Fig. 16a. The expected power from the fuel cell should be 4.2W at a current of 1.7A.

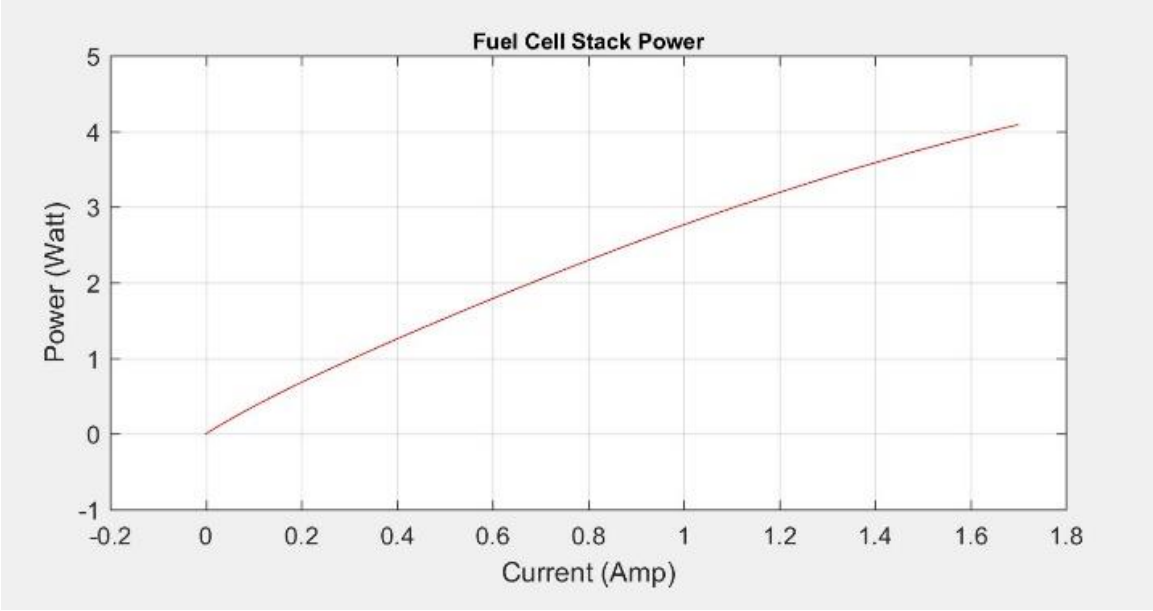

Figure 16a: Plot of Power and current from the whole fuel cell stack

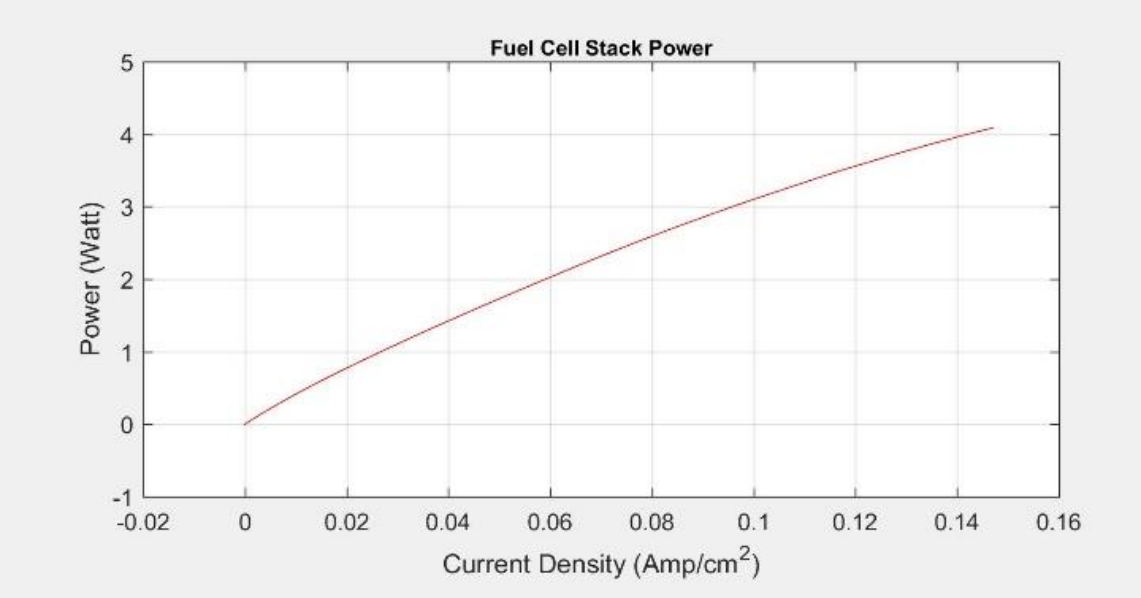

Figure 16b: Plot of Power and current from the whole fuel cell stack

Dividing the whole power for the entire stack by the number of cells in the stack leads to the generation of the power for just one stack as shown on Fig. 17a. Again it can be seen that an increase in the current yields a power of 0.82W at a current density of 1.7. Fig. 17b shows a plot of current density of the single stack versus the power of the stack.

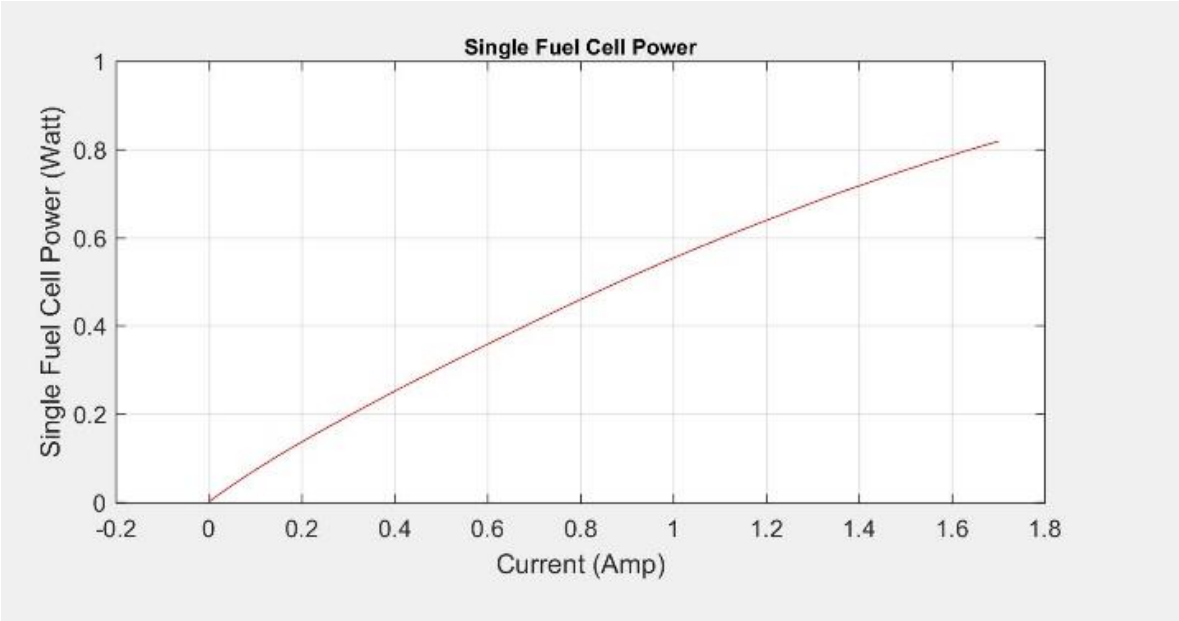

Figure 17a: Plot of Power and current from one cell stack.

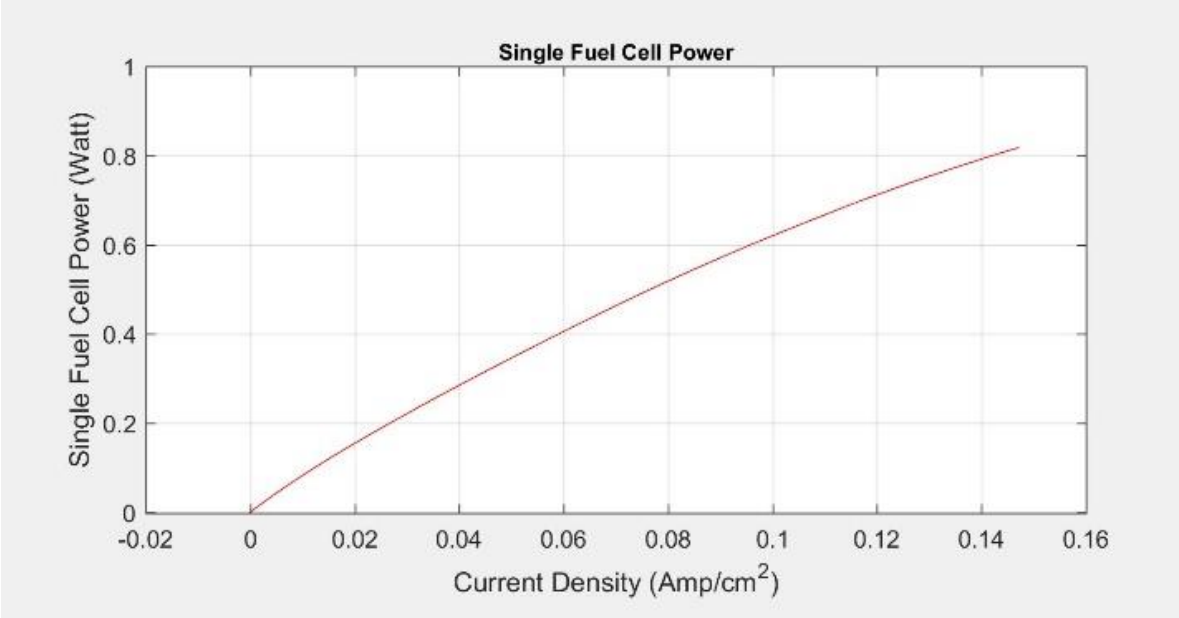

Figure 17b: Plot of Power and current from the one cell stack.

Efficiency is usually defined in two ways:

$$\eta_{\Delta G} = \frac{\text{actual useful work}}{\text{maximum useful work}} = \frac{\text{Power x time}}{\Delta \text{G}} \tag{26}$$

$$\eta_{\Delta H} = \frac{\text{actual useful work}}{\text{maximum useful work}} = \frac{\text{Power x time}}{\Delta \text{H}} \tag{27}$$

It is anticipated that an efficient fuel cell should have its efficiency between 60 and 90% under standard conditions where ΔG = -237.2 kJ/mol and ΔH = - 285.8kJ/mol [25, 26] where the efficiency of the fuel cell is given by $\eta_{\text{fuel-cell}} = \Delta G / \Delta H$.

The fuel cell transforms chemical energy into electrical energy. The maximum theoretical efficiency can be calculated using the following equations:

$$\eta_{\text{m}} = 1 - T^* \frac{\Delta S}{\Delta H} \tag{28}$$

As long as the fuel cell operates reversibly and isothermally it will have efficiency between 60% and 90%. From Fig. 18, the efficiency of the fuel cell will be nearly 70% but once current is being drawn gradually from the cell this efficiency begins to drop gradually. At very high current, the efficiency is lower.

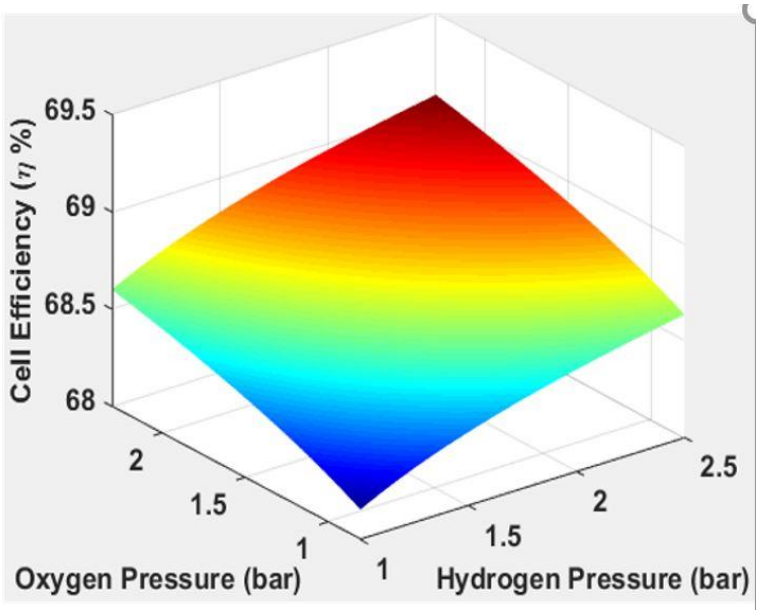

Figure 18: Fuel cell stack Efficiency

Fig. 19 shows the waste heat generated by the entire stack. As the current density increases, the waste heat generated by the stack increases.

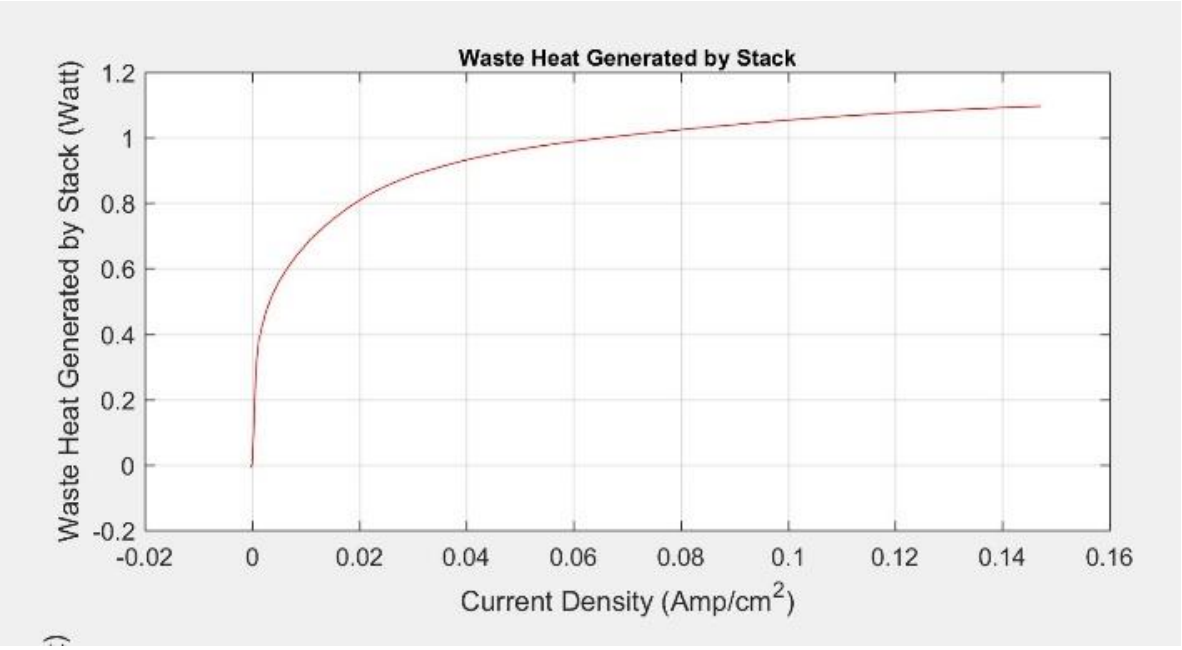

Figure 19a: Waste Heat Generated by the stack

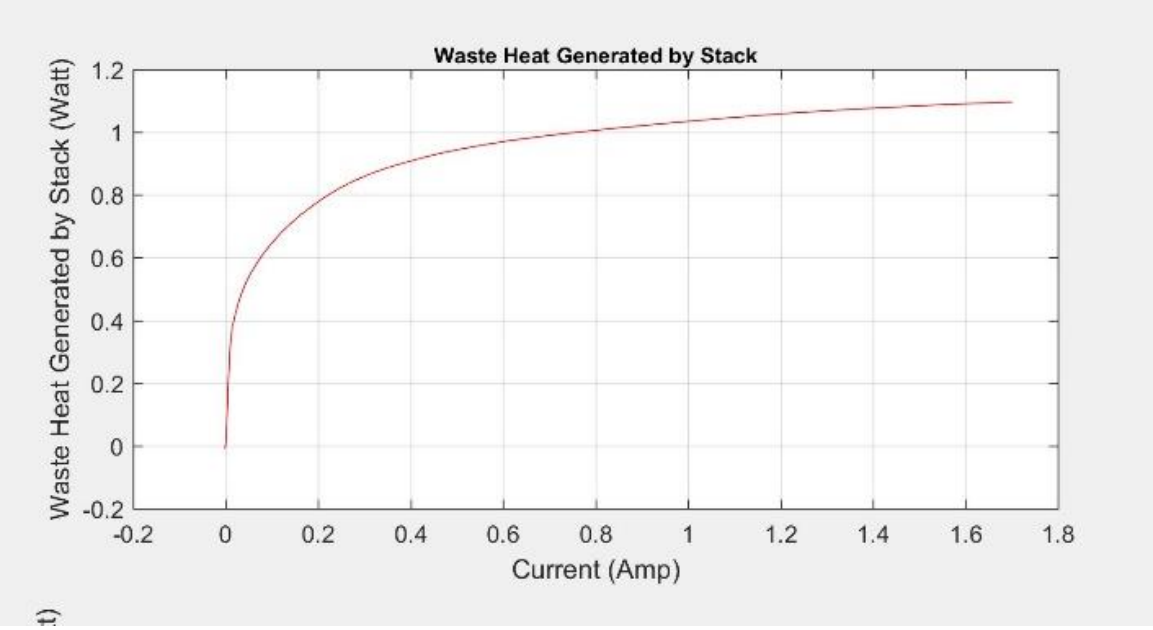

Figure 19b: Waste Heat Generated by the stack

Effect of operating pressure on the performance of the fuel cell without humidification

The experiment conducted in this part aimed to maintain a constant air flow rate entering the fuel cell while varying the pressure of the fuel entering the cell at the anode section. The hydrogen gas was supplied to the fuel cell in a dead end mode and the flow rate of the hydrogen gas was not controlled but only measured. From the graph, the open circuit voltage that was recorded for the four experiments showed that the maximum voltage that could be generated from the fuel cell being tested was 4.11V at the highest operating pressure of 2.5bar. There were some inconsistencies in the open circuit voltage for the 4 experiments conducted but the results showed that an increase in the pressure of the reactive gas resulted in increased voltage output as indicated by the graphs in Fig. (20). Once the fuel cell started generating current, it is noticed that there is a sudden drop in voltage and these were highly inconsistent for all the experiments conducted. This could be explained as the membrane of the fuel cell was drying up and the air entering the fuel cell at random occasions due to movement within the room. The mass transport phenomenon occurring in the cell was also inconsistent and subsequently contributed to the sudden rise and fall of the voltage being generated from the fuel cell under these conditions.

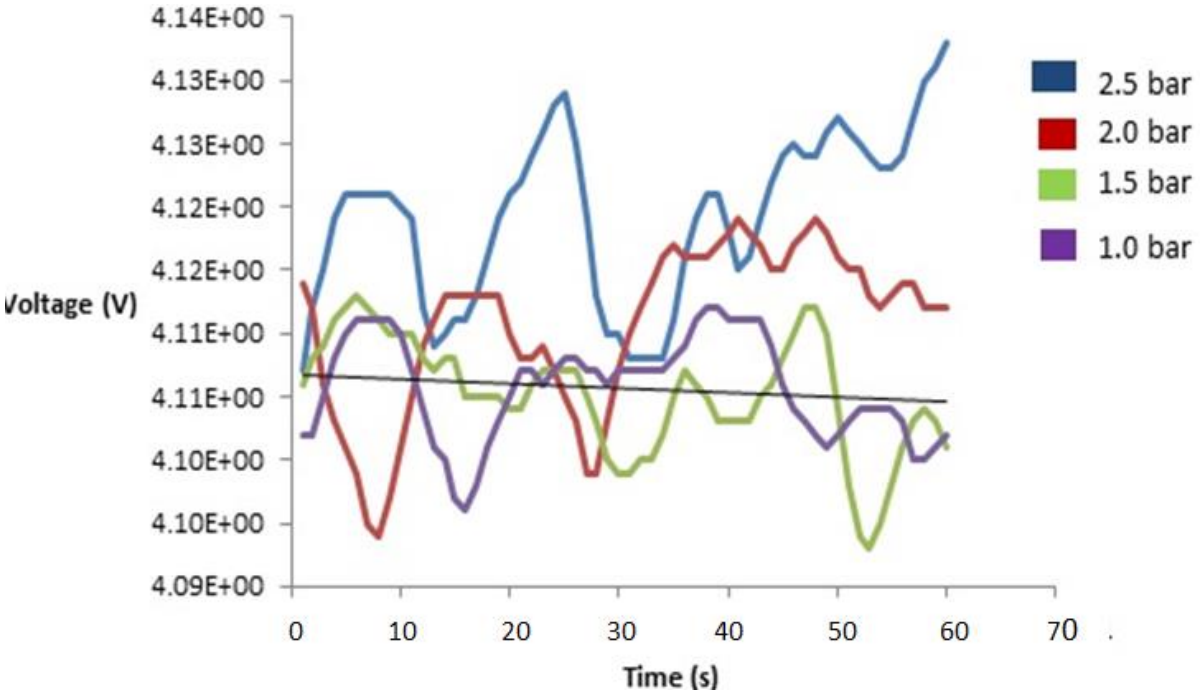

Figure 20: Polarization curve for the performance of the fuel cell at different operating temperatures

Effect of pressure on the open circuit voltage of fuel cell with humidification of the fuel (Hydrogen).

The next experiment conducted was to check the effect of keeping the hydrogen gas humidified but with no fan attached to the fuel cell. With pressure being varied, the polarization curve showed that the open circuit voltage increases appreciably to 4.5V for all the experiments conducted, clearly confirming the importance of humidification on the performance of the fuel cell. The fuel cell once humidified was generating nearly 6A of current and again the activation polarization is noticed to be almost constant at the onset of the fuel cell producing current but the curves deviated from each other at higher current densities. The voltage also drops once the fuel cell starts generating current till it reaches the maximum current the fuel cell can produce. At that maximum point the voltage becomes zero and that is the limiting current density.

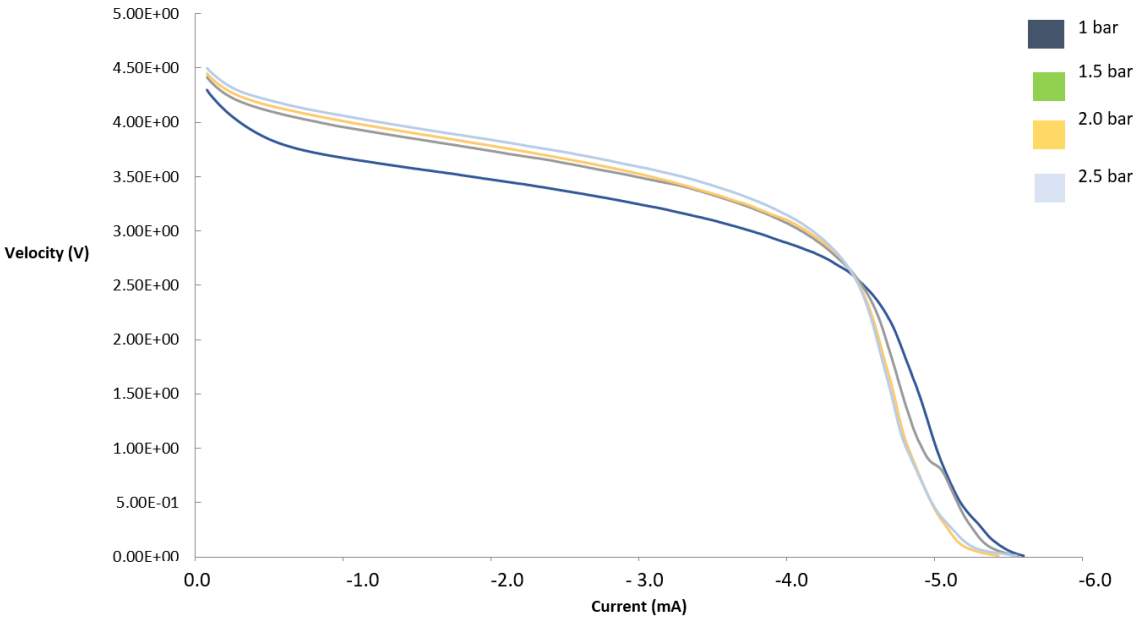

Figure 21: Polarization curve for the performance of the fuel cell with humidified hydrogen gas

A surface plot was also generated to show the maximum current and voltage that could be generated from the fuel cell at varying cell temperatures and pressures. Fig. 22 shows the result at a constant temperature of 40°C and varying pressure.

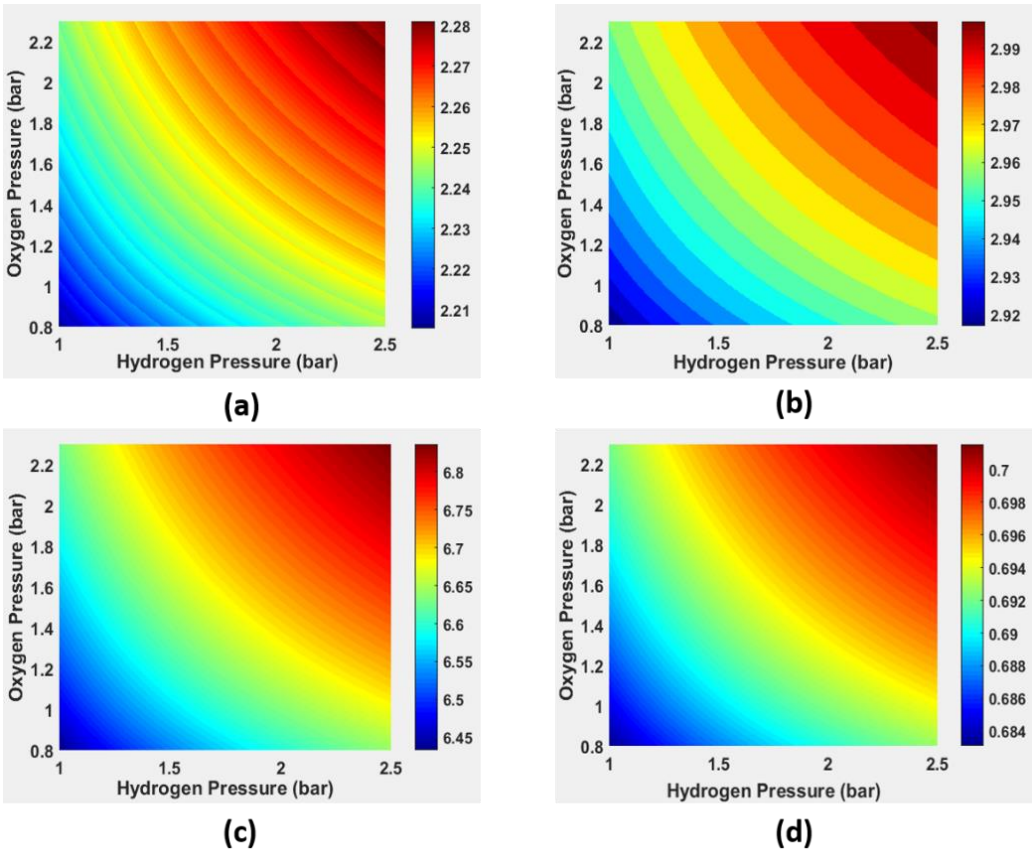

Figure 22. (a) Stack voltage (V) (b) Stack current (A) (c) Maximum Stack Power (W) (d) Fuel Cell efficiency – Constant temperature of 40°C

It can be seen that the maximum stack voltage can be generated from the fuel cell operating at its maximum operating pressure for both the fuel and the air but it is also possible to generate the maximum voltage at a combination of low hydrogen pressure and high oxygen pressure which will be more economical (Fig. 22(a)). The same could be said for the current, power as well as the efficiency of the fuel cell itself.

Another experiment that was conducted was to vary the cell operating temperature with respect to oxygen pressure by increasing the speed of the fan and also the distance between the fan and the fuel cell to determine the maximum voltage, current, power and the fuel cell efficiency; and the results are shown in Fig. 23. It is also observed that high oxygen pressure gave the maximum fuel cell performance as could be seen from the surface plot.

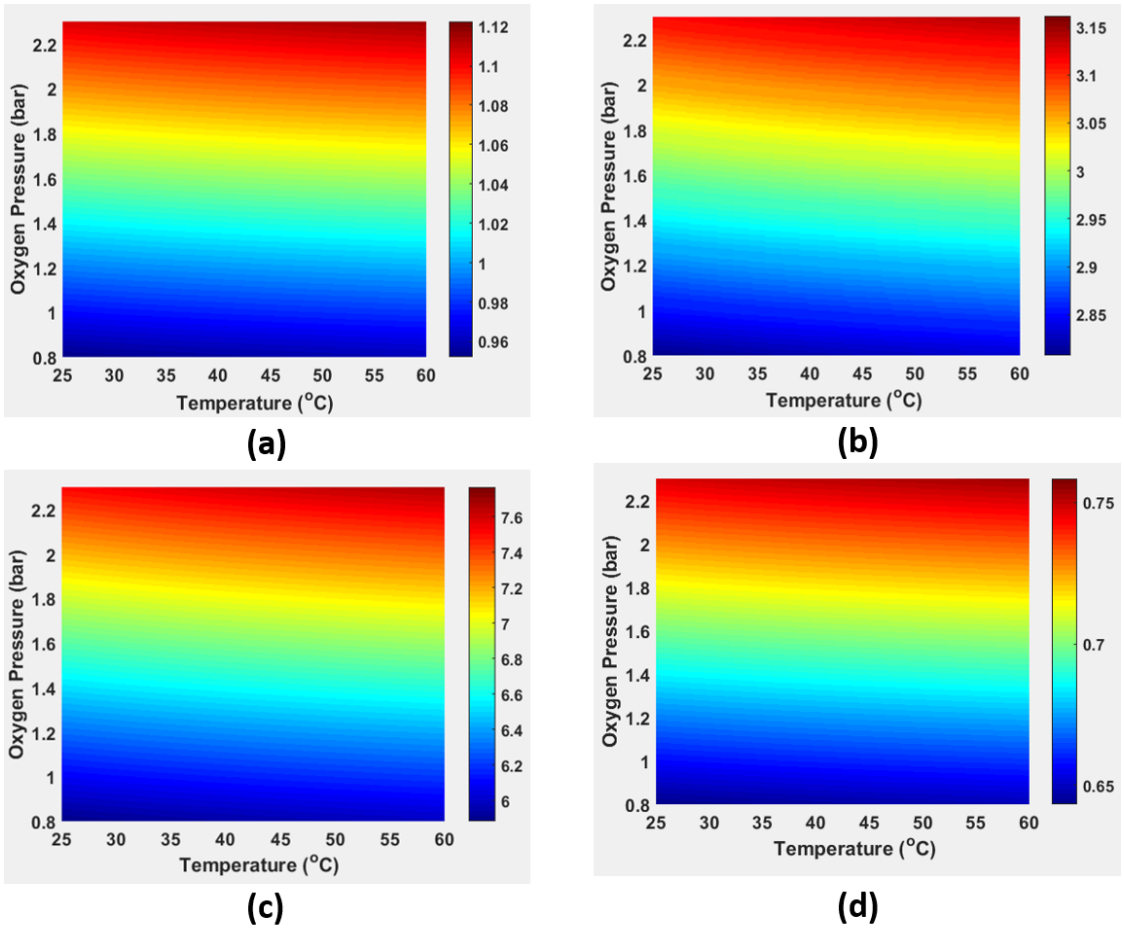

Figure 23 (a) Open circuit Cell Voltage (V) (b) Stack Current (A) (c) Maximum power (W) (d) fuel cell efficiency – Constant hydrogen pressure of 2.5 bar

The effects of varying the pressures of hydrogen and oxygen simultaneously on current, voltage, power and cell efficiency are also studied Fig. 24 shows the 3D surface plot of these effects at the maximum power of the fuel cell. Again it is noticed that the performance of the cell was highly dependent on the oxygen pressure or conditions around the cathode region.

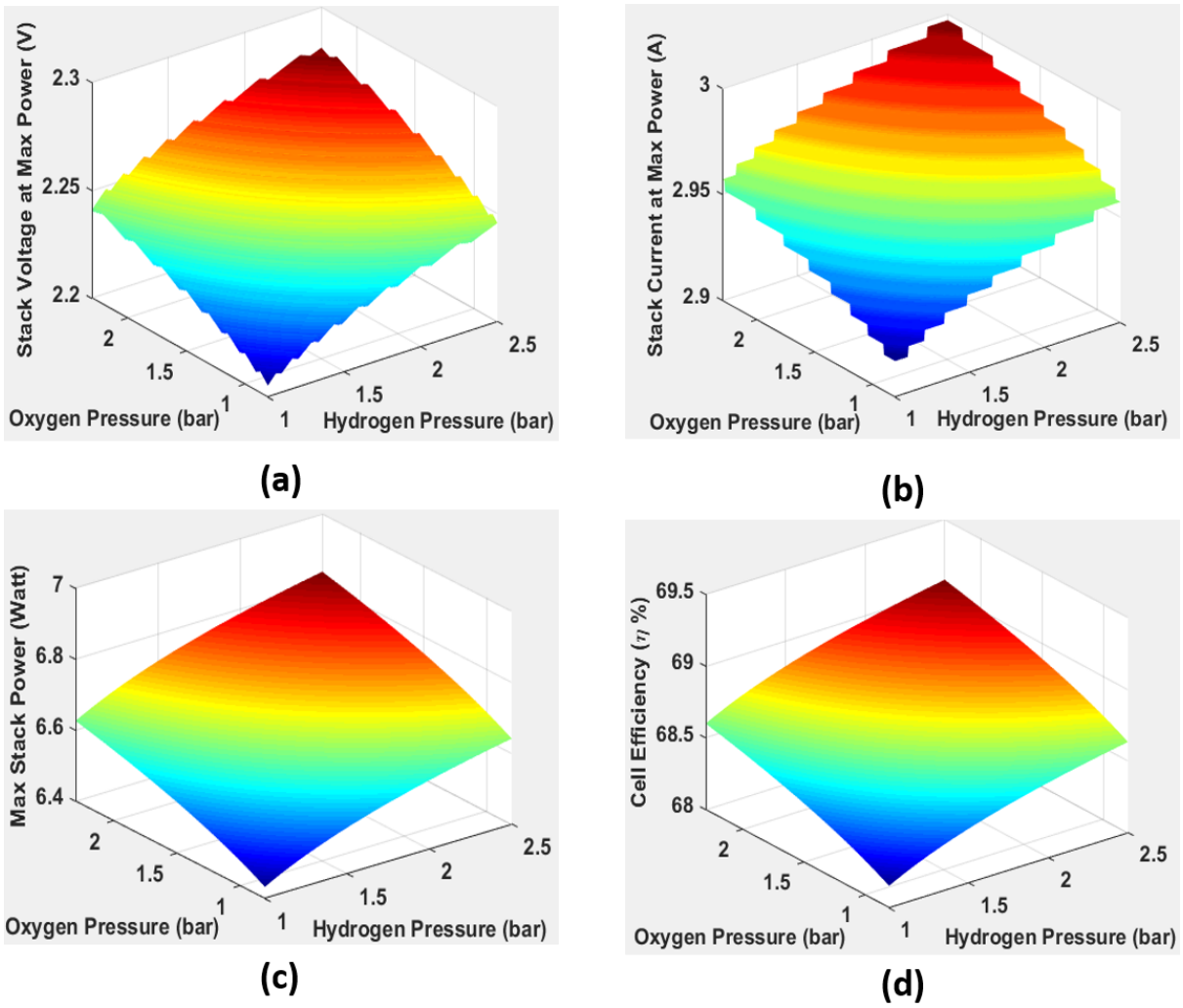

Figure 24 (a) Open circuit Cell Voltage (V) (b) Stack Current (A) (c) Maximum power (W) (d) fuel cell efficiency – Constant hydrogen pressure of 2.5 bar

Effect of operating temperature on the performance of the fuel cell

The performance of the fuel cell was evaluated with the fuel humidified at certain specific operating temperatures ranging from room temperature in the laboratory at 18^{o}C to 47^{o}C. It is noticed from the graph that the performance of the fuel cell increased appreciably. The open circuit voltage increased to almost 4.7V compared with the other polarization curves where the open circuit voltage was 4.1V without humidification at maximum temperature. It was also observed that at room temperature the corresponding voltage with humidification was 4.4V. The voltage increment due to the increase in temperature can be results of several possible effects such an increase in the gas diffusivity and membrane conductivity at higher temperatures and this eventually affects the current being generated from the fuel cell due to reduction in the activation losses. Also as the temperature increases, there is the possibility of increased rate of surface reaction with the increased temperature. Another observation made

was that at extremely high temperatures above 55°C, the performance of the fuel cell began to deteriorate. This was caused by the decrease in membrane conductivity hence there was a significant drop in relative humidity of the reactant gases and the water content in the membrane [25-30]. This explains that between 50°C and 60°C the performance of the fuel cell is likely to drop from the values shown in Fig (25). Evaporation increases with increased temperature and the physical adsorption rate is also predicted to decrease. So as the operating temperature of the fuel cell increases, the rate of water evaporation from the membrane also increases. This phenomenon leads to higher resistivity in the cell.

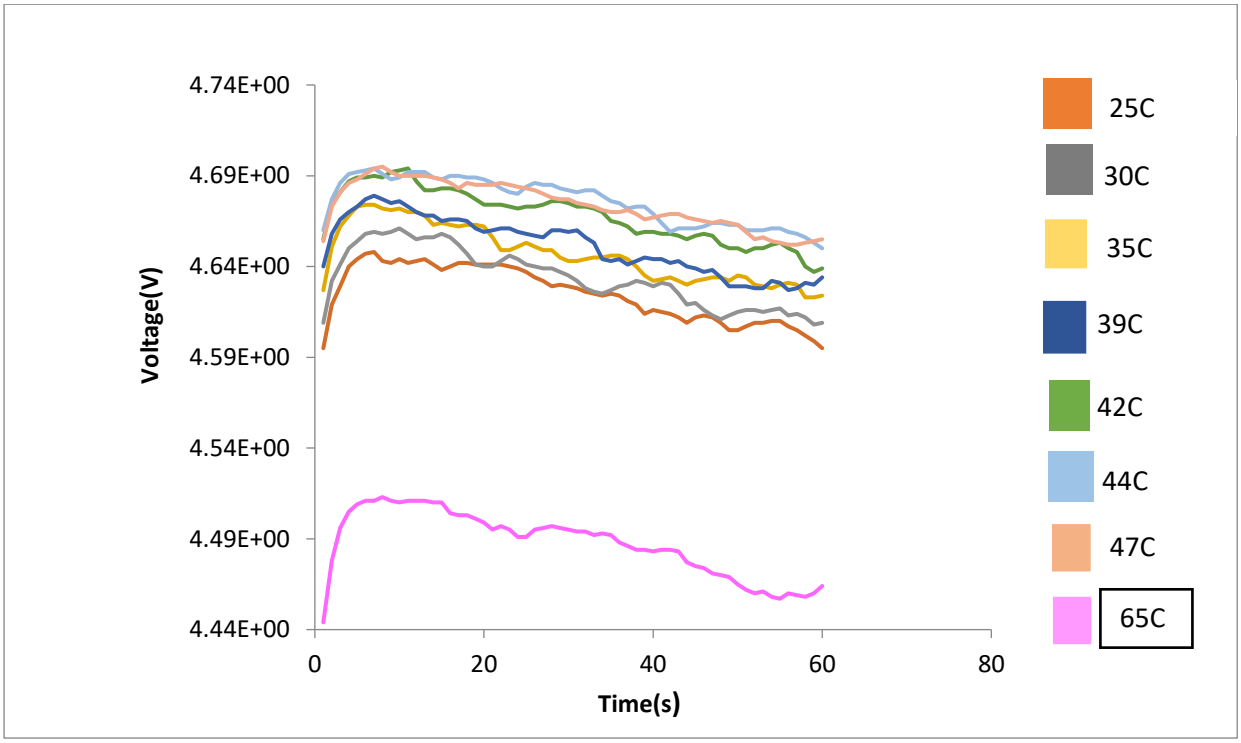

Figure 25: The effect of operating temperature of the cell on the performance of the entire fuel cell stack

Effects of humidification temperature on the characteristic performance of the fuel cell

Another experiment that was carried out in this report was the performance of the fuel cell based on humidification temperatures. The operating temperature of the fuel cell was varied between 18°C to 47°C and the humidification chamber had its temperature increased between 30°C and 80°C using a hot plate. The operating temperature of the cell was kept constant prior to the start of this experiment at a higher temperature between 50 and 65°C whiles the temperature of the humidification chamber was increased to a maximum of 80°C. It was observed that between room temperature of 18 and 47°C the fuel cell characteristics were the

same as there were high increases in performance with increased cell operating temperature and humidification temperature as explained earlier. The major change observed was at high temperatures between cell operating temperature of 50°C and 65°C and humidification above 70°C. Unlike previously observed results; where, at higher cell operating temperatures the performance dropped due to higher evaporation rate of membrane water, increasing resistivity in the membrane electrode assembly; the fuel cell performed well at higher cell operating temperature due to the increased humidification temperature as shown in Fig. 26. This in effect increased the amount of current being generated from the fuel cell as well.

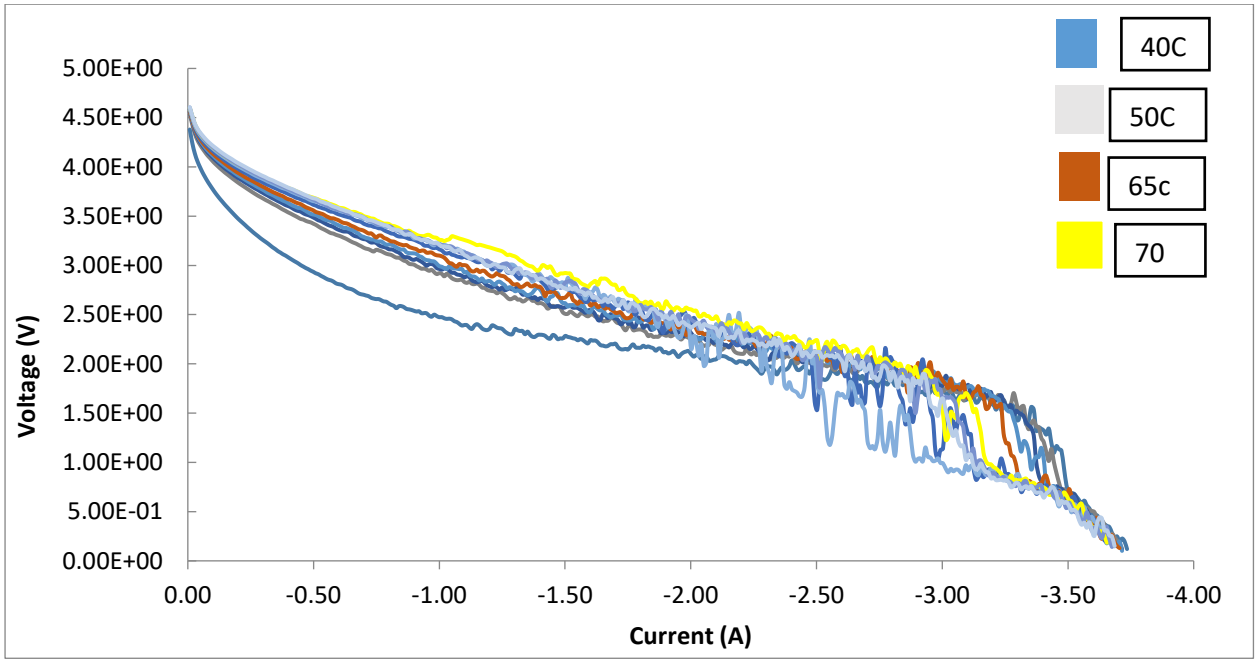

Figure 26: Polarization curve for the performance of the fuel cell at high cell operating temperature and high humidification.

Fundamental principle behind this phenomenon

Several factors affect the reactor performance irrespective of the operating conditions. All catalytic reactions on solid surfaces involve several steps such as:

1. Diffusion from the fluid bulk to the outer surface of the catalyst.
2. Diffusion into the catalysts pores.
3. Adsorption of the reactants onto the active sites
4. Surface reaction
5. Desorption of products from the active sites.
6. Diffusion of products away from inside the catalyst pores towards the catalyst outer surface.
7. Diffusion of products from the catalyst outer surface into the bulk of the fluid.

The overall rate of reaction is limited by the slowest process among the above steps.

The rate of reaction is commonly expressed using the power law formulae.

For the reaction:

$$aA + bB \rightarrow Products \tag{29}$$

The reaction rate can be written as:

$$(-r_A) = A_o e^{-E/RT} C_A^a C_B^b \tag{30}$$

The frequency factor (A_o) and the activation energy (E) are dependent on the catalyst.

Adsorption Isotherm

An adsorption isotherm is the relationship at constant temperature between the partial pressure of the adsorbate above the catalyst and the amount adsorbed. It varies from 0 at P/P_o = 0 to infinity as P/P_O reaches 1 assuming the contact angle with the surface is zero i.e completely wetted or the occurrence of condensation. The shape of the isotherm also varies depending on the adsorbate. Hysteresis loops are often formed for substances with fine pores with capillary condensation. Physical adsorption is almost the same as condensation of vapour molecules onto liquids of the same composition. This is often caused by van der waals

forces such as dipole-dipole or induced dipole forces. Solid catalysed reactions normally occur at temperatures higher than the boiling point of the reactants and chemisorption tends to be primarily responsible. Physical adsorption precedes chemisorption and helps in pore condensation that helps bring molecules closer together in a quasi – liquid state leading to chemisorption. The value of physical adsorption is limited in catalytic reactions but could help in determining catalyst surface area, void fraction and pore size distribution [30, 31].

Chemisorption

Chemisorption involves chemical bonding and it is very similar to chemical reactions. There is transfer of electrons between the adsorbate and the adsorbent in chemisorption. Many forms of chemisorption may exist but like chemical reactions the rates of the different forms become significant when the conditions are suitable. In most catalytic processes the reaction takes place at temperatures far higher than the boiling point of the reactants. Forces involved in physical adsorption are much weaker than the ones encountered in chemical bonding and can't possibly cause distortion of force fields around the molecules [30]. The rate of chemical adsorption of reactants or desorption of products studied individually may indicate the slow and therefore rate-limiting step in the catalytic cycle. They may also help characterize surface heterogeneity.

Physical adsorption does not require activation energy and can occur as soon as molecules strike the surface. Chemisorption requires activation energy and the process is often slower than physical adsorption. In the case of chemisorption, at lower temperatures, more time is needed in order to reach equilibrium. Chemisorption is also more substantial than physical adsorption above the boiling point of the adsorbate or its critical point [31-34].

The membrane used for this experiment was a sulfonated perfluoropolymer (Sp) membrane specifically Nafion 212. Nafion membranes have high protonic conductivity and chemical stability. Zawodzinski et al, 1993 [35] explained that the water concentration in a membrane determined the protonic conductivity of the membrane. However Nishikawa et al. [36] also reported that the general water holding capacity of every membrane should be known as too much humidification would lead to a reduction of the catalytic activity and flooding in the gas diffusion layer particularly at the cathode of the fuel cell. Water molecules are transported from the anode to the cathode with proton and this transport phenomenon is called electro osmotic drag. The proton, electron and oxygen generate the water at the cathode. Electro-osmotic drag and water generation reaction cause the gradient of water

concentration across the membrane and water molecules are transported from the cathode to the anode by diffusion. The circulation of water in the membrane greatly affects the performance of the fuel cell hence the need for it to be quantified. The water concentration in the membrane determines the electro-osmotic drag coefficient and the diffusion coefficient. Ye and Le Van [37] compared the diffusion coefficient of water in the membrane as reported by other researchers. The first step in order to determine the water concentration dependence of the electro-osmotic drag coefficient and the diffusion coefficient of water in the membrane is the determination of the adsorption properties of water vapour on the membrane. The equilibrium vapour pressure was determined from the volume fraction of the solvent by Futerko [38] using the Flory Huggins equation [39] and his results were in perfect agreement with the data reported. Springer et al. [40-47] and Hinatsu [48] obtained the water adsorption isotherms equations at 30°C and 80°C respectively. The thermodynamics theory and the adsorption isotherm equation of water vapour on Nafion 212 were also discussed by Choi [49]. The modified B.E.T equation was also used by Tsonos [38] but the results were not in perfect agreement at higher humidity (90%). The adsorption isotherm equation should ideally include both the partial pressure of water vapour and the temperature for calculating the amount of adsorbed water under various conditions.

Adsorption model of water vapour on the membrane

The clustering theory from the statistical molecular distribution was developed by Zimm and Lundberg [41] using the equation below:

$$\frac{G_{WW}}{V_W} = -(1-\varphi_W)\left[\frac{\partial\left({}^{a_w}/_{\varphi_w}\right)}{\partial aw}\right]_{p,T} - 1 \tag{31}$$

$$\varphi_W = 1 - \varphi_P \tag{32}$$

Where:

$\frac{G_{WW}}{V_W}$ = clustering function

a_w = water vapour activity

φ_w = volume fraction of water in the binary system

The mean cluster size of water was estimated by using Eq. (33):

$$MCS = 1 + \left[\frac{\varphi_{WG_{WW}}}{V_W}\right] \tag{33}$$

This equation is often used to determine the mean number of clustered water molecules.

Flory – Huggins theory

The theory developed by Florry [39] and Huggins [42] gives the relationship of the water vapour activity, a_w to the volume fraction of the solvent, φ_W as shown in the Eq. (34):

$$lna_w = ln\varphi_W + \left(1 - \frac{1}{r}\right)(1 - \varphi_W) + X[(1 - \varphi_W)^2] \tag{34}$$

$$r = \frac{V_P}{V_W} \tag{35}$$

Where:

X = Polymer-solvent interaction parameter

r = ratio of molar volume of polymer, V_p (cm^3/mol) and the molar volume of water V_w (cm^3/mol)

All these equations were used by Futerko [38] as well as Arce et al. [43] to fit the water adsorption isotherm for Nafion 117. Futerko [38] concluded that the adsorption of water on the membrane was highly dependent on the temperature. Including the partial pressure of water vapour and temperature in the adsorption equation would have shown the effect on the mass transport in the gas film and in the membrane.

Multi – mode adsorption

Barrer et al. [44] investigated the adsorption isotherms of different types of hydrocarbons in ethyl cellulose. He noted that the adsorption isotherm can be described using the Freundlich equation. The report further stated that the dual- mode adsorption isotherm combined Langmuir and Henry equations in order to theoretically explain the adsorption phenomenon in cellulose. The dual mode adsorption isotherm equation is as shown in equation xx.

$$Q_h = \frac{abP_h}{1 + bP_h} + kP_h \tag{36}$$

Where:

Q_h (g/cm^3) = amount of adsorbed hydrocarbon (Solvent)

a(g/cm^3) and b (Pa^{-1}) = Langmuir parameters

k (g/cm^3) = Henry parameters

P_h (Pa) = partial pressure of hydrocarbons

The dual mode of equation to express the sigmoid adsorption isotherm of water vapour by adding the clustering term was developed by Park [45]. The water molecules adsorbed according to the Henry's law make clusters but it was first hypnotized. He represented the clustering reaction of water using:

$$\mathrm{n}H_2\mathrm{O} \overset{K}{\leftrightarrow} (H_2O)_n \tag{37}$$

$$K = \frac{[(H_2O)_n]}{[H_2O]^n} \tag{38}$$

where:

n = mean number of water molecules in a cluster

K = Equilibrium constant which can also be expressed by:

$$K = \frac{[(H_2O)_n]}{K^n P_w^n} \tag{39}$$

Where P_w (Pa) = partial pressure of water vapour

The amount of adsorbed water Q (g/cm^3) using the multi – mode equation can therefore be given by:

$$Q = \frac{abP_w}{1 + bP_w} + KP_w + \frac{KK^nP_W}{n} \tag{40}$$

The water adsorption of the SP membrane was studied in detail by Dellante et al [46] using the multi-mode equation including the partial pressure of water vapour and the temperature as parameters. He argued that the value of K was not temperature dependent but in reality all equilibrium constant for any reaction is temperature dependent.

Finite layer B.E.T equation for clustering model

Fig. 27 represents the adsorption model on a finite layer according to the model developed by Takata et al. [47] and other researchers [45 -56]. Their model was generated assuming the vapour adsorbs on the membrane forming a monolayer with Langmuir adsorption then followed by water vapour clusters on the monolayer.

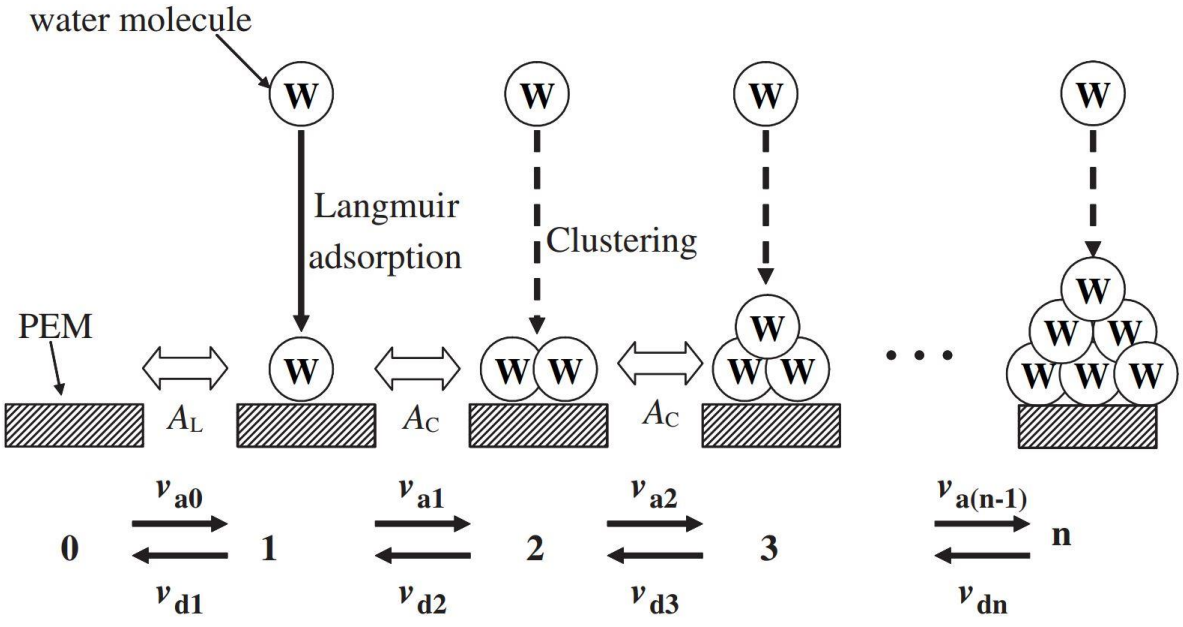

Figure 27: Adsorption model of water vapour on membrane [47]

They stated the adsorption rate and desorption rate as $v_{an}\,(mol/s)$ and $v_{dn}\,(mol/s)$, respectively and these rates were also expressed by:

$$v_{(a)0} = k_{a0}\,\theta_0 P_w \tag{41}$$

$$v_{(d1)} = k_{d1}\theta_1 \tag{42}$$

Where:

k_{a0} (mol/s Pa) = Proportionality constant for adsorption

k_{d1} (mol/s) = Proportionality constant for desorption rate

Pw (Pa) = Partial pressure of water

θ_0 = fraction of vacant adsorption site

θ_1 = fraction of occupied adsorption site by monomolecular layer

At equilibrium the rate of adsorption and desorption are considered to be at equilibrium hence:

$$\theta_1 = \frac{k_{a0}}{k_{d1}}\,\theta_0 P_W = A_L \theta_0 P_W \tag{43}$$

$$A_L = A_{L0}\,\exp\left(-\frac{E_L}{RT}\right) \tag{44}$$

Where:

A_L= Equilibrium constant between 0_{th} and 1_{st} layer (Pa^{-1})

A_{L0} = Frequency factor of A_L

E_L = Activation Energy of Langmuir type adsorption

R = Gas constant (J/mol K)

T = Temperature (K)

The relationship between θ_0 and θ_1 is given below.

$$\theta_1 + \theta_o = 1 \tag{45}$$

Saturated amount of monolayer is defined as B_L(g/cm^3 – dried membrane) therefore amount of water absorbed by the monolayer is:

$$Q_L = B_L \theta_1 \tag{46}$$

Adding up all the equations together:

$$Q_L = \frac{A_L B_L P_W}{(1 + A_L P_W)} \tag{47}$$

From the 1st and 2nd layer of the membrane, the same equations are used:

$$\theta_2 = \frac{k_{a1}}{k_{d2}} \theta_1 P_W = A_c \theta_1 P_W \tag{48}$$

$$A_c = A_{c0} \exp\left(-\frac{E_c}{RT}\right) \tag{49}$$

Where:

A_c= Equilibrium constant between 1st and 2nd layer (Pa^{-1})

A_{c0} = Frequency factor of A_c

E_c = Activation Energy of Langmuir type adsorption (J/mol K)

R = Gas constant (J/mol K)

T = Temperature (K)

Takat et al [47] therefore derived the adsorption equation considering the nth term of the membrane layer as:

$$Q = Q_L + Q_C \tag{50}$$

$$Q = Q_L + Q_C = \frac{A_l B_L P_w}{(1 + A_L P_w)}[1 + (n-1)(A_C P_w)^{n-1}] \tag{51}$$

A relation that was also deduced and this was:

$$lnQ_C = (n-1)lnP_w + Const. \tag{52}$$

At high humidity range the clustering reaction have an impact on the amount of water adsorbed on the membrane [48-51]. The curve fitting parameters that were proposed by Takata et al. [47] for other temperatures were:

$$B_L = 0.160 \tag{53}$$

$$n = 5.15 \tag{54}$$

The parameters A_C and A_L can also be derived using the equations below:

$$A_L = 1.53 \times 10^{-10} exp\left(\frac{39000}{RT}\right) \tag{55}$$

$$A_C = 2.40 \times 10^{-10} exp\left(\frac{39000}{RT}\right) \tag{56}$$

The adsorption isothermal equation derived was:

$$Q = \frac{2.45X10^{-11}\exp\left(\frac{39000}{RT}\right)P_W}{\left[1 + 1.53X10^{-10}\exp\left(\frac{39000}{RT}\right)P_W\right]\left[1 + 2.49X10^{-48}\exp\left(\frac{190900}{RT}\right)P_W^{4.15}\right]} \quad (57)$$

From all the equation above it is obvious that a rise in humidity temperature will eventually affect the general performance of the fuel cell irrespective of the cell operating temperature. This in effect contributed to the better performance of the cell at high humidity temperature of 65°C though the operating temperature was high.

Effect of using pure oxygen and hydrogen as reactive substance

An experiment was also performed using pure oxygen as the reactive substance for the cathodic reaction. This experiment was conducted to investigate the impact of using pure oxygen instead of air on the polarization curve. The experiment was conducted for 50 cycles using the Gamry potentiostat. The cell operating temperature was carefully monitored during the experiment and it was observed that the operating temperature of the fuel cell often rise from room temperature of 18°C and increases to 33°C. After the first experimental cycle, the operating temperature was 27°C and maintained a constant rise to 33.7°C, 33.3°C, 32.1°C, 30.7°C and 29.3°C for the 20th, 30th, 40th and 50th cycle of the experiment. The drop in operating cell temperature was as the result of the production of water as the various reactive substances go into reaction.

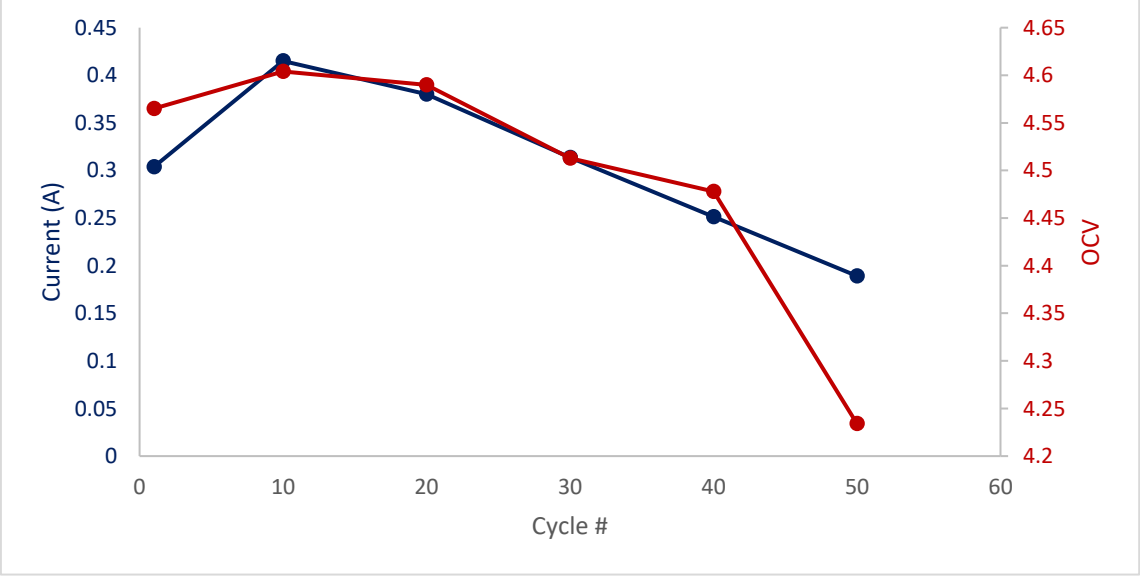

Figure 28: Polarization curve for the number of experimental cycles, current and voltage.

From the polarization curve, the current generated by the fuel cell increases appreciably but after the 10th cycle, the performance of the fuel cell began to drop. This is because of the drying up of the membrane as the cell operating temperature increased resulting in higher resistance in the membrane leading to reduction in protonic conductivity. It was also observed that the open circuit voltage also drops from the 1st experimental cycle to the 50th experimental cycle. A solution to keeping the performance of the fuel cell high is to increase the temperature of the humidification chamber. This will in effect maintain the performance of the fuel cell for a period of time.

Fig. 29 shows the performance of the fuel cell with respect to temperature and as explained earlier increasing the temperature of the fuel cell will over a period of time reduce the performance of the fuel cell once the membrane begins to dry up.

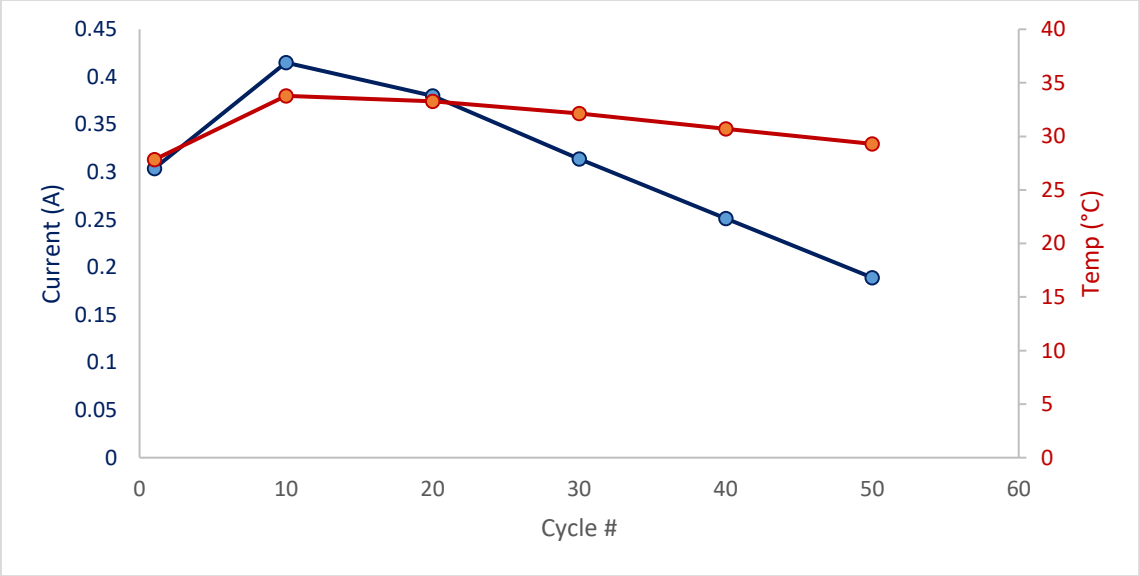

Figure 29: Polarization curve for the effect of temperature on the amount of current generated from the fuel cell.

Every fuel cell has its breaking point where its performance begins to drop and exceeding this point eventually causes the performance of the fuel cell to reduce. The experiment exposed the need for all researchers to first know the maximum operating temperature the fuel cell membrane can hold before conducting any experiment. The fuel cell performance dropped after the 50th cycle because the membrane at this point was almost dried as shown in Fig (30).

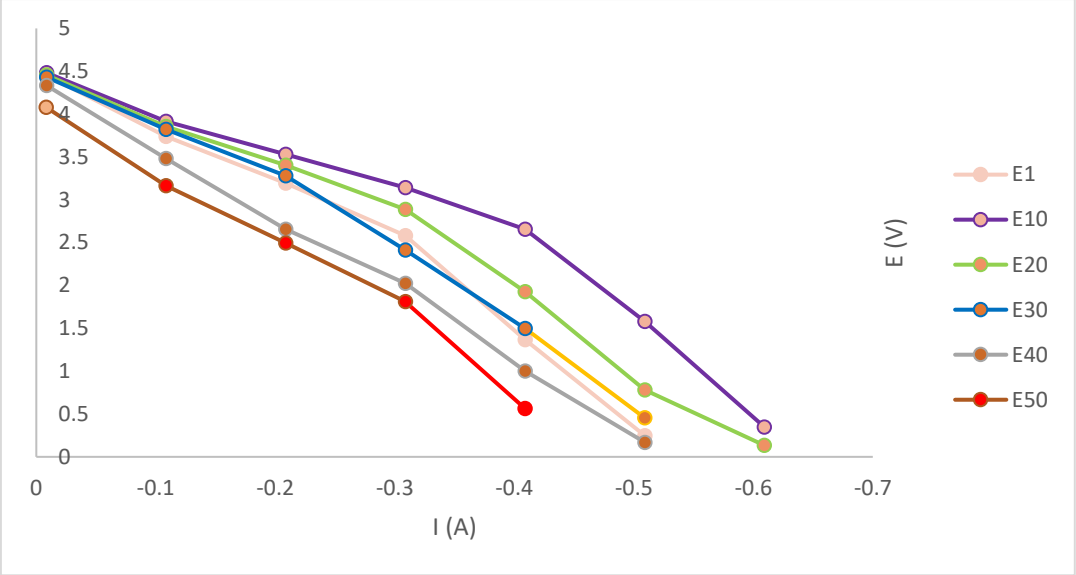

Figure 30: The performance of the fuel cell using pure oxygen with respect to the number of cycles.

Losses in the fuel cell with respect to temperature

Another experiment that was conducted during the investigation was to keep the reactant pressures constant but vary the cell temperature. This was to give a clear idea of the best operating cell temperature that could aid in generating the maximum power from the fuel cell as shown in Fig. 31.

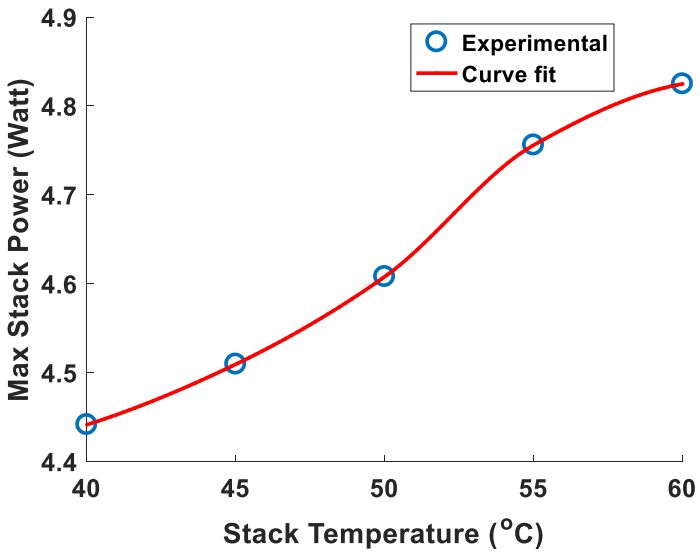

Figure 31: Effect of increasing stack temperature to the maximum achievable power from the PEM FC Stack at hydrogen pressure of 2.5 bar.

With this determined, all the losses experienced in the fuel cell as the temperature increased were analysed carefully. From figure 30, it is also observed that the activation polarization reduced as the temperature of the cell increased. This contributes to the reason for the fuel cell performing better at high temperatures. At 25ºC, the activation polarization was 0.015V as compared to the activation polarization at 60ºC which was 0.149V. The ohmic potential at that maximum power region was seen to be constant but the concentration loss also increased as the temperature increased as shown in Fig. 32.

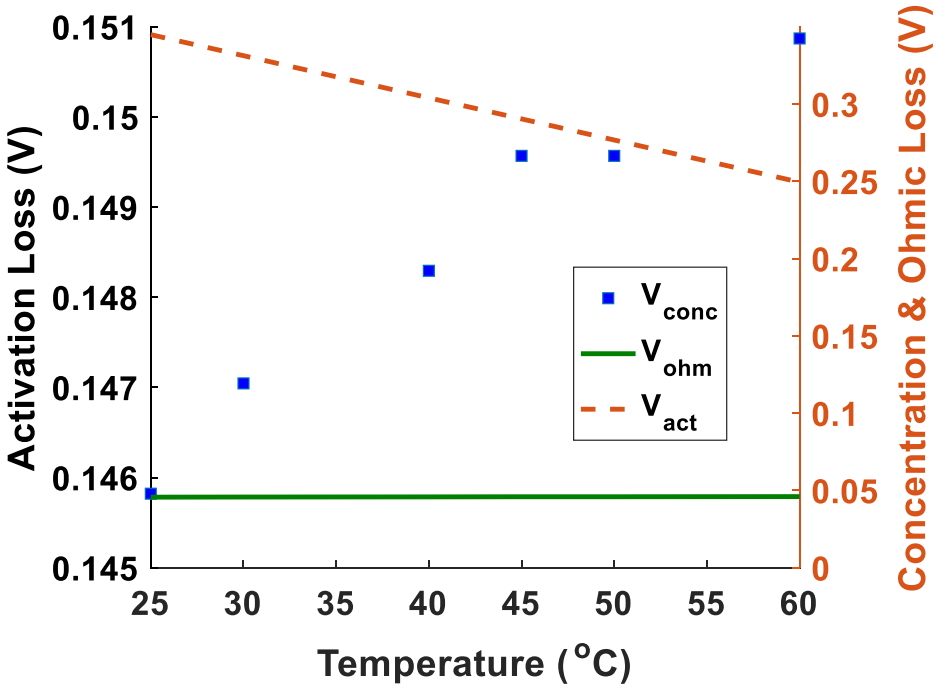

Figure 32: Loss characteristics at maximum power over a range of increasing cell temperature

Conclusion

This work reports on the study of the effects of several factors on the performance of PEM fuel cells and the optimization of these parameters to improve the performance of the fuel cells. The plotting of the various polarization curves in MATLAB helped facilitate the analysis of the various conditions occurring in the fuel cell. The work was also able to establish the levels of hydrogen consumption as well as the oxygen consumption that are needed for any reactive process in a fuel cell to improve the efficiency of the entire process.

The work showed that increasing the flow rate of the oxygen (or air) while keeping the hydrogen flow rate constant increased the voltage appreciably. Various over-potentials contributed to the reduction in voltages that occur at open circuit voltages. Activation losses, ohmic losses and concentration losses were some known over-potentials that occurs in the fuel cell. Another observation was that increasing the current or current density reduced the voltage. The amount of water generated as a result of the various reactions occurring in the fuel cell increased when the current being generated from the fuel cell increased. The efficiency of the fuel cell declined when the current increased. The study also analysed the effect on the humidification temperature on the performance of the fuel cell.

Finally, at a constant reaction pressure but varying cell temperatures, the activation losses increased appreciably whiles the ohmic losses remained constant at the maximum operational conditions. The concentration loss also increased marginally as temperature increased. This shows that the cell operating temperature was one of the key contributors to the performance of the cell and the performance of a cell operating at a lower temperature was compared with that of a cell operating at higher temperatures.

Reference

1. Tabbi Wilberforce, A. Alaswad, A. Palumbo, A. G. Olabi. Advances in stationary and portable fuel cell applications. International Journal of Hydrogen Energy 41(37) March 2016.
2. Tabbi Wilberforce, Ahmed Al Makky, A. Baroutaji, Rubal Sambi, A.G. Olabi. Computational Fluid Dynamic Simulation and modelling (CFX) of Flow Plate in PEM fuel cell using Aluminum Open Pore Cellular Foam Material. Power and Energy Conference (TPEC), IEEE, Texas. 2017. DOI: 10.1109/TPEC.2017.7868285.
3. Tabbi Wilberforce, Ahmed Al Makky, A. Baroutaji, Rubal Sambi, A.G. Olabi Optimization of bipolar plate through computational fluid dynamics simulation and modelling using nickle open pore cellular foam material. International conference on reneable energies and power quality (ICREPQ'17), ISSN 2171-038X, No 15 April 2017
4. Tabbi Wilberforce, Abed Alaswad, A.G. Olabi. Improving flow plate design in fuel cell. Poster presentation, RSC Scotand and North of England Regional Electrochemistry Symposium, April, 2016.
5. Tabbi Wilberforce, A. Alaswad, J. Mooney, A. G. Olabi. Hydrogen Production for Solar Energy Storage. A Proposed Design Investigation. Proceedings of the 8th International Conference on sustainable Energy and Environmental Protection. ISBN: 978-1-903978-52-8.
6. Carton, J. G., Olabi, A. G. Representative model and flow characteristics of open pore cellular foam and potential use in proton exchange membrane fuel cells. International Journal Of Hydrogen Energy 40 (2015) 5726 – 5738.
7. Carton, J. G., Olabi, A. G. Wind/hydrogen hybrid systems: opportunity for Ireland's wind resources to provide consistent sustainable energy supply. Energy 2010:35(12): 4536 – 44.
8. Olabi AG. The 3rd international conference on sustainable energy and environmental protection SEEP 2009 the guest editor's introduction. Energy 2010;35:4508-9
9. Baroutaji, A., Carton, G. J., Olabi, A. G. Design and development of Proton Exchange Membrane Fuel Cell Using Open Pore Cellular Foam as Flow Plate Material. Journal of Energy Challenges and Mechanics. Volume 1 (2014) issue 2, article.
10. Alaswad A, Palumbo A, Dassisti M, Olabi AG. PEM fuel cell cost analysis during the period. In: Accepted in reference module in materials science and materials engineering (MATS). All rights reserved: 2016 Elsevier Inc; 1998-2014.

11. Lister, S., and G. Mclean. PEM fuel cell electrode: A review .J.Power Sources. Vol 130, 2004, pp. 61-76
12. Matsumoto, T., T. Komatsu, K. Arai, T. Yamazaki, M. Kijima, H. Shimizu, Y. Takasawa, and J. Nakamura. Reduction of Pt usage in fuel cell electrocatalysts with carbon nanotube electrodes. Chem. Commun. 2004, pp. 840–841.
13. Morita, H., M. Komoda, Y. Mugikura, Y. Izaki, T. Watanabe, Y. Masuda, and T. Matsuyama. Performance analysis of molten carbonate fuel cell using a Li/Na electrolyte. J. Power Sources. Vol. 112, 2002, pp. 509–518.
14. Silva, V.S., J. Schirmer, R. Reissner, B. Ruffmann, H. Silva, A. Mendes, L.M. Madeira, and S.P. Nunes. Proton electrolyte membrane properties and direct methanol fuel cell performance. J. Power Sources. Vol. 140, 2005, pp. 41–49.
15. You, L., and H. Liu. A two-phase fl ow and transport model for PEM fuel cells. J. Power Sources. Vol. 155, 2006, pp. 219–230.
16. Coutanceau, C., L. Demarconnay, C. Lamy, and J.M. Leger. Development of electrocatalysts for solid alkaline fuel cell (SAFC). J. Power Sources. Vol. 156, 2006, pp. 14–19.
17. Li, X., and I. Sabir. Review of bipolar plates in PEM fuel cells: Flow-fi eld designs. Int. J. Hydrogen Energy. Vol. 30, 2005, pp. 359–371.
18. Fabian, T., J.D. Posner, R. O'Hayre, S.-W. Cha, J.K. Eaton, F.B. Prinz, and J.G. Santiago. The role of ambient conditions on the performance of a planar, air-breathing hydrogen PEM fuel cell. J. Power Sources. Vol. 161, 2006, pp. 168–182.
19. Lin, B. 1999. Conceptual design and modeling of a fuel cell scooter for urban Asia. Princeton University, master's thesis.
20. Song, R.-H., and D.R. Shin. Infl uence of CO concentration and reactant gas pressure on cell performance in PAFC. Int. J. Hydrogen Energy. Vol. 26, 2001, pp. 1259–1262.
21. Li, Xianguo. Principles of fuel cells. 2006. New York: Taylor & Francis Group.
22. Stolten, D. 2012. Fuel cells and Engineering. Materials, Process, systems and technology. Volume 1. Wiley – VCH Verlag GmbH & Co. KGaA.
23. Barbir F. PEM fuel cells: theory and practice. USA: Elsvier Academic Press: 2005
24. O'Hayre R, Cha S, Colella W, Prinz FB. Fuel cell fundamentals. USA: John Wiley and Sons: 2006.
25. Chen, E., Thermodynamics and Electrochemical kinetics, in G. Hoogers (editor) Fuel cell Technology Handbook. Boca Raton, FL: CRC Press, 2003.

26. Colleen, S. S., Designing & Building of fuel cell, 1st ed. ISBN 0-07-148977-0, McGraw – Hil, 2007.
27. A.G. Olabi, 2016, Hydrogen and Fuel Cell developments: An introduction to the special issue on "The 8th International Conference on Sustainable Energy and Environmental Protection (SEEP 2015), 11-14 August 2015, Paisley, Scotland, UK", *International Journal of Hydrogen Energy*, 41, pp.16323-16329.
28. Colleen, S. S., PEM Fuel Cell, Modelling, Simulation Using MATLAB. ISBN 978-0-12-374259-9, Academic Press, 2008.
29. Mench, M.M., Z.H. Wang, K. Bhatia, and C.Y Wang. Design of a Micro – direct Methanol Fuel cell. Electrochemical Engine Centre, Department of Mechanical and Nuclear Engineering, Pennsylvania State University. 2001.
30. Springer et al. Polymer Electrolyte Fuel cell Model.
31. A.G.Olabi, 2016, Energy quadrilemma and the future of renewable energy, *Energy*, 108, pp 1-6.
32. Subash, Singhall C. High Temperature Solid Oxide fuel cells fundamentals, Design and Applications. PanAmerican Advanced Studies Institute. Rio de Janeiro
33. C. N. Satterfield, Heterogeneous Catalysis in Industrial Practice, 2nd Ed, McGraw Hill, 1991.
34. A. Foley and A. G.Olabi, 2017, Renewable energy technology developments, trends and policy implications that can underpin the drive for global climate change, *Renewable and Sustainable Energy Reviews*,68(2017)1112–1114.
35. Zawodzinski Jr. TA, Springer TE, Davey J, Jestel R, Lopez C, Valerio J. et al. A comparative study of water uptake by and transport through ionomeric fuel cell membranes. J Electrochem Soc 1993;140:1981–5.
36. Nishikawa M, Takeishi T, Enoeda M, Higashijima T, Munakata K, Kumabe I. Catalytic oxidation of tritium in wet gas. J Nucl Sci Technol 1985;22:922–33.
37. Ye X, Levan MD. Water transport properties of Nafion membranes part I. Single-tube membrane module for air drying. J Membr Sci 2003;221
38. Futerko P, Hsing IM. Thermodynamics of water vapor uptake in perfluorosulfonic acid membranes. J Electrochem Soc 1999;146: 2049–53.
39. Flory PJ. Principles of polymer chemistry. Ithaca, NY: Cornell University Press; 1953.
40. Springer TE, Zawodzinski TA, Gottesfeld S. Polymer electrolyte fuel cell model. J Electrochem Soc 1991; 138:2334–42.

41. Zimm BH, Lundberg JL. Sorption of vapors by high polymers. J Phys Chem 1956; 60:425–8.
42. Huggis M.L.Thermodynamic Properties of Liquids, Including Solutions. IX. Thermodynamic Properties of Polymer Solutions. *Polymer Journal* (1973) **4,** 502-510; doi:10.1295/polymj.4.502
43. Arce A, Fornasiero F, Rodriguez O, Radke CJ, Prausnitz JM. Sorption and transport of water vapor in thin polymer films at 35 ◦C. Phys Chem Chem Phys 2004;6:103–8.
44. Barrer RM, Barrie JA, Slater J. Sorption and diffusion in ethyl cellulose Part III. Comparison between ethyl cellose and Rubber. J Polym Sci 1958;27:177–97.
45. Park GS. Transport principles—solution, diffusion and permeation in polymer membranes, in: Bungay PM (Ed.), Synthetic membranes, science engineering and applications. Dordrecht: D. Reidel Publishing Company; 1986, p. 57–107.
46. Detallante V, Langevin D, Chappy C, Metayer M, Mercier R, Pineri M. Water vapor sorption in naphthalenic sulfonated polyimide membranes J Membr Sci 2001;190:227–41.
47. Takata H, Nishikawa M, Arimura Y, Egawa T, Fukada S, Yoshitake M. Study on water uptake of proton exchange membrane by using tritiated water sorption method. Int J Hydrogen Energy 2005; 30:1017–25.
48. Hinatsu JT, Mizuhata M, Takenaka H. Water uptake of perfluorosulfonic acid membranes from liquid water and water vapor. J Electrochem Soc 1994; 141:1493–8.
49. Choi P, Jalani NH, Datta R. Thermodynamics and proton transport in Nafion I. Membrane swelling, and ion-sorption, and ion-exchange equilibrium. J Electrochem Soc 2005; 152:E84–9.
50. Tsonos C, Apekis L, Pissis P. Water sorption and dielectric relaxation spectroscopy studies in hydrated Nafion_ (−SO3K) membranes. J Mater Sci 2000;35:5957–65
51. Anderson RB. Modification of the Brunauer Emmett and Teller equation. J Am Chem Soc 1946; 68:686–91.
52. Gates CM, Newman J. Equilibrium and diffusion of methanol and water in a Nafion 117 membrane. AIChE J 2000; 46:2076–85.
53. Morris DR, Sun X. Water-sorption and transport properties of Nafion 117 H. J Appl Polym Sci 1993; 50:1445–52.
54. Guo X, Fang J, Tanaka K, Kita H, Okamoto K. Synthesis and properties of novel sulfonated polyimides from 2, 2-bis(4-aminophenoxy)biphenyl- 5, 5_-disulfonic acid. J Polym Sci Part A: Polym Chem 2004;42: 1432–40.

55. Lundberg JL. Molecular clustering and segregation in sorption systems Pure Appl Chem 1972; 31:261–81.
56. Favre E, Schaetzel P, Nguygen QT, Clement R, Neel J. Sorption, diffusion and vapor permeation of various penetrants through dense poly (dimethylsioxane) membranes: a transport analysis. J Membr Sci 1994;92:169–84